THE SEC6/8 (A.K.A. EXOCYST) COMPLEX SUPPORTS DNA REPAIR FIDELITY

APPROVED BY SUPERVISORY COMMITTEE

Michael White, Ph.D (Mentor)

Rolf Brekken, Ph.D (Chair)

Sandeep Burma, Ph.D

Melanie Cobb, Ph.D

Acknowledgements

I would like to thank my mentor Dr. Michael White for allowing me to opportunity to learn from his successes and become a stand-alone scientist. I would like to also thank my committee for their openness to my studies and behind-the-scenes support as I pursued my research endeavors. I would like to thank my mother and father for instilling in me the value of pursuing higher education and facilitating my abilities to do so. Finally, I would like to thank my wife, Valerie, who has endured a long road with me and supported me to the end.

THE SEC6/8 (A.K.A. EXOCYST) COMPLEX SUPPORTS DNA REPAIR FIDELITY

by

MICHAEL JASON TORRES

DISSERTATION

Presented to the Faculty of the Graduate School of Biomedical Sciences

The University of Texas Southwestern Medical Center at Dallas

In Partial Fulfillment of the Requirements

For the Degree of

DOCTOR OF PHILOSOPHY

The University of Texas Southwestern Medical Center at Dallas

Dallas, Texas

April, 2014

THE SEC6/8 (A.K.A. EXOCYST) COMPLEX SUPPORTS DNA REPAIR FIDELITY

MICHAEL JASON TORRES

The University of Texas Southwestern Medical Center at Dallas, 2014

Supervising Professor: MICHAEL A WHITE, Ph.D

The exocyst complex, first described in yeast, is a heterooctomeric complex that serves as a signaling platform to mediate cellular responses to diverse spatial and temporal cues. Evidence suggests that the exocyst might contribute to oncogenesis, potentially by disrupting spatial and temporal regulation of pathways critical to determining cell survival vs. apoptosis. Our work investigated how cancer cells subvert the exocyst to upregulate the AKT (v-akt murine thymoma viral oncogene) pro-survival pathway through the innate immune protein TBK1 (TANK-binding kinase 1). siRNA-mediated depletion of TBK1 in pancreatic and breast cancer cell lines results in apoptosis, which is mediated through the AKT pathway. Pharmacological inhibition of TBK1 recapitulates the apoptotic phenotype in mouse

orthotopic models. Additionally, my work uncovered exocyst participation in the regulation of DNA repair. The isolation of multiple components of the DNA damage response (DDR) within the human exocyst protein-protein interaction network, together with the identification of Sec8 as a suppressor of the p53 response, prompted an investigation of functional interactions between the exocyst and the DDR. We found that exocyst perturbation resulted in a radioresistance phenotype to ionizing radiation (IR) that was associated with accelerated resolution of DNA damage. This occurred at the expense of genomic integrity, as enhanced recombination frequencies correlated with the accumulation of aberrant chromatid exchanges. Exocyst-dependent modulation of the DDR is, at least in part, through restraint of the associated chromatin modifiers ATF2 and RNF20. Exocyst perturbation resulted in aberrant accumulation of ATF2 and RNF20; the promiscuous accumulation of DDR-associated chromatin marks; and IR-induced increased Rad51 repairosomes. Thus, the exocyst indirectly supports DNA repair fidelity by limiting formation of repair chromatin in the absence of a DNA damage signal. This newly revealed regulation of DNA repair by the exocyst may provide additional insight into the emerging observations of DNA damage protein involvement in pathways not canonically associated DNA repair, such as the host cytokinesis, host defense response, and maintenance of cilia. This work further substantiates the importance of the exocyst in normal cell biology and gives insight into how disruption of exocyst function can result in disease.

TABLE OF CONTENTS

PRIOR PUBLICATIONS

Torres, MJ Pandita, K, Kukak O, Kumar R, Formstecher E, Zhao Y, Lum L, Pandita TK, White M. The Sec6/8 (a.k.a. Exocyst) Complex Supports DNA Repair Fidelity. (In prep.)

Ou, Y.-H., **Torres, M**., Ram, R., Formstecher, E., Roland, C., Cheng, T., et al. (2011). TBK1 Directly Engages Akt/PKB Survival Signaling to Support Oncogenic Transformation. *Molecular Cell*, *41*(4), 458–470. doi:10.1016/j.molcel.2011.01.019

Shimura, T., **Torres, M. J**., Martin, M. M., Rao, V. A., Pommier, Y., Katsura, M., et al. (2008). Bloom's syndrome helicase and Mus81 are required to induce transient double-strand DNA breaks in response to DNA replication stress. *Journal of molecular biology*, *375*(4), 1152–1164. doi:10.1016/j.jmb.2007.11.006

Shimura, T., Martin, M. M., **Torres, M. J.**, Gu, C., Pluth, J. M., DeBernardi, M. A., et al. (2007). DNA-PK is involved in repairing a transient surge of DNA breaks induced by deceleration of DNA replication. *Journal of molecular biology*, *367*(3), 665–680. doi:10.1016/j.jmb.2007.01.018

LIST OF FIGURES

LIST OF DEFINITIONS

53BP1- p53-binding protein 1

ATM- Ataxia Telangiectasia mutated

ATR- Ataxia Telangiectasia and Rad3 related

AKT- RAC-alpha serine/threonine protein kinase

APH- Aphidicolin

ATF2- Activating transcription factor 2

ATP- Adenosine Triphosphate

BECN- Coiled-coil myosin-like BCL2-interacting protein

CAK- CDK-activating kinase

CDC42- Cell division Cycle 42

CDT1- Chromatin licensing and DNA replication factor 1

CEP- Centrosomal protein

CldU- 5-Chloro-2′-deoxyuridine

CRC- Colorectal Cancer

DAPI- 4',6-diamidino-2-phenylindole

DDR- DNA damage response

DSB- Double stranded break

EXOC- Exocyst component

EGF- Epidermal growth factor

FACs- Fluorescence-activating cell sorting

FANC- Fanconi Anemia

GFP- Green fluorescent protein

GSK3- Glycogen synthase kinase 3

H2AX- H2A histone family, member X

H2B- H2B histone

HAT- Histone acetyltransferase

HBEC- Human bronchial epithelial cell

HPA2- Histone acetyltransferase HPA2

HR- Homologous recombination

HU- Hydroxyurea

HUWE1- HECT, UBA and WWE domain containing 1, E3 ubiquitin protein ligase

IdU- 5-Iodo-2′-deoxyuridine

IFNb- Interferon beta 1, fibroblast

IKKe- IKK-related kinease epsilon

IP- Immunoprecipitation

IRF- Interferon regulatory factor

IR- Irradiation

KAT5- K(lysine) acetyltransferase 5

KAT8- K(lysine) acetyltransferase 8

LC3- Microtubule-associated protein 1 light chain 3 alpha

LPS- Lipopolysaccharide

MEF- Mouse embryo fibroblast

MKLP1- Mitotic kinesin-like protein 1

MPM2- Mitotic protein 2

MS- Mass Spectrometry

mTOR- mammalian target of rapamycin complex 1

NHEJ- Non-homologous end joining

NSCLC- Non-small cell lung cancer

p53- Tumor protein p53

PCNT- Pericentrin

PDK1- Pyruvate dehydrogenase kinase, isozyme 1

PI- Propidium Iodide

PI3K- Phosphatidylinositol-4,5-bisphosphate 3-kinase

PKD- Polycystic Kidney Disease

PKD2- Polycystic kidney disease 2 (autosomal dominant)

PPI- Protein-protein interaction

PRKDC- Protein kinase, DNA-activated, catalytic polypeptide

PRPF19- Pre-mRNA processing factor 19

PTMs- Post-translational modifications

Rad51- RAD51 recombinase

Ral- Ras-like GTPase

RalGDS- Ral guanine nucleotide dissociation factor

RalGEF- Ral-specific Guanyl nucleotide exchange factor

Ras- Rat sarcoma viral oncogene

Rho- Rhodopsin

RNF- Ring finger protein

Sec-Secretory mutant

SGA- Synthetic genetic array

siRNA- Small interfering RNA

TBK1- Tank binding kinase 1

TC-NER- Transcription-Coupled Nucleotide Excision Repair

Tip60 (KAT5)- Histone acetyltransferase Tip60

TMEM173- Transmembrane protein 173

UBR5- Ubiquitin protein ligase E3 component n-recognin 5

ULK1- Unc-51-like kinase 1

Y2H- Yeast Two Hybrid

CHAPTER ONE
The Exocyst Complex

Introduction

The heterooctomeric exocyst complex is an evolutionarily conserved protein machine that was first identified in yeast by mutational studies that looked for defects in exocytosis[1]. Initial characterization of the yeast exocyst complex firmly placed the exocyst in the vesicle trafficking pathway, serving to direct post-Golgi vesicles to targeted domains of the plasma membrane[2]. Beyond yeast, the importance of the exocyst complex is underscored by the lethality in development that occurs in *Drosophila* and mice with exocyst subunit deletions[3,4]. Mutations in the exocyst have also been coupled to human disease[5-7].

Structure and Function of the Exocyst Complex

In yeast, the proteins identified as the exocyst complex are known as Sec8, Sec6, Sec5, Exo70, Exo84, Sec3, Sec10, and Sec15. In mammalian cells, the exocyst complex proteins are known as Exoc1, Exoc2, Exoc3, Exoc4, Exoc5, Exoc6, Exoc7, Exoc8. The exocyst complex proteins consist of helical bundles that are thought to assemble into a rod-like structure as evidenced by electron microscopy[8]. Within the rod-like structure of the exocyst as a whole, there are distinct domains on individual exocyst subunits that help to specify interaction, and thus function, of the exocyst complex. For instance, there is genetic evidence for functional interaction with the small GTPase family of proteins, and this evidence was enhanced by the crystallization of the RalA GTPase with Sec5 and Exo84[9]. Also, the yeast Sec3 subunit contains a novel Pleckstrin Homlogy domain that interacts with small GTPases

and with P(4,5)P[10]. The interactions with small GTPases have been shown to facilitate signaling cascades that are mediated by exocyst interaction. However, questions remain to how the exocyst is assembled and dissembled and if there are subcomplexes of particular exocyst proteins that respond to specific instructive signals, such as nutrient sensing.

One biological context, in which the exocyst participates in, is the autophagy regulatory network. Work from our lab showed specific contributions of exocyst subcomplexes in response to nutrient availability. In nutrient-rich conditions, mTORC1 (mammalian target of rapamycin complex 1), a master regulator of the cellular response to nutrient availability[11], interacts with a Sec5 subcomplex that promotes inactivation of ULK1 (Unc-51-like kinase 1), a key kinase that which promotes autophagy[12]. Conversely, in nutrient-deficient conditions, in a RalB-dependent manner, an Exo84 subcomplex, promotes the activation of ULK1 and facilitates assembly of autophagy machinery[13]. Thus, in response to nutrient availability, context-specific exocyst subcomplexes are mobilized and facilitate an appropriate response to cellular cues.

The exocyst has also been shown to function in cytokinesis. The exocyst complex localizes at the midbody ring in a centriolin dependent manner. This localization facilitates the delivery of vesicles to the midbody ring. These exocyst directed vesicles are then fused to the plasma membrane and mark the site for abscission and final completion of cytokinesis[14].

The exocyst complex has also been shown to be important in maintaining cellular polarity by mediating the effects of the polarity regulators Rho and Cdc42 in driving polarization of actin cytoskeleton for vesicle delivery to distinct plasma membrane domains[15,16].

Additional functions for the exocyst have been uncovered include directing membrane expansion in cell migration and ciliogenesis[17,18]. Thus, the exocyst supports diverse functions within cells to direct vesicles to specific membrane domains and to support signaling events by facilitating interactions with between proteins.

Exocyst Complex and Disease

Given the wide variety of cellular contexts in which the exocyst plays a critical function, it is not surprising that exocyst mutations are associated with human disease diagnoses. Recent evidence has implicated Sec8 as being a potential driver of a rare, lethal ciliopathy named Meckel-Gruber Syndrome[6]. This disease is characterized by renal cystic dysplasia, occipital encephalocele, polydactyly (post axial), hepatic developmental defects, and pulmonary hypoplasia. It is interesting to note that some centrosome proteins that are associated with milder forms of ciliopathies have been shown to interact with the exocyst[19].

There is also strong evidence linking the exocyst to oncogenesis and cancer cell survival. Mutations of members of the exocyst complex have been associated with driving oncogenesis. In a large scale study examining mutational profile of several breast and colorectal cancers, Sec8 was identified as being frequently mutated, suggesting that Sec8

may play a role in cancer initiation or progression[20]. Another study examined tumors of African Americans with colorectal cancer and found Sec8 deletion in 80% of the tumors[7].

Overexpression of exocyst components have also been associated with tumorigenic behavior. Sec8 was found to be overexpressed in oral squamous-cell carcinoma and associated with increased invasion by secretion of matrix metalloproteinases, such that inhibition of Sec8 in this context reduced cell proliferation and invasion[5].

Beyond mutations within the exocyst complex itself, dysregulation of proteins that interact with the exocyst often depend on the exocyst to exert their oncogenic properties. As an example, oncogenic Ras (Rat sarcoma viral oncogene) can drive Ral (Ras-like GTPase) activity, with the exocyst being a Ral effector[21]. One study sought to determine candidates that drive Ral-mediated tumor cell survival by an RNAi-based candidate screen of RalGTPase effector proteins and found Sec5 as being necessary for this event[22]. Furthermore, inhibition of Exo84 reduced oncogenic RalGEF-mediated transformation and oncogenic Ras-driven tumorigenic growth of human cells[23]. Thus, observations suggest that not only is the exocyst itself important in maintaining tumor suppressive activities, but that aberrant signaling events that drive oncogenic effects can be mediated by the exocyst, as well.

Therefore, as an important platform for signaling, it is essential to understand the biological context and functions of the exocyst within those contexts to determine whether there are novel functions for the exocyst as a spatial and temporal signaling platform. The purpose of

this study is to examine exocyst depletion within selective biological contexts to determine how exocyst complex dysregulation promotes oncogenesis.

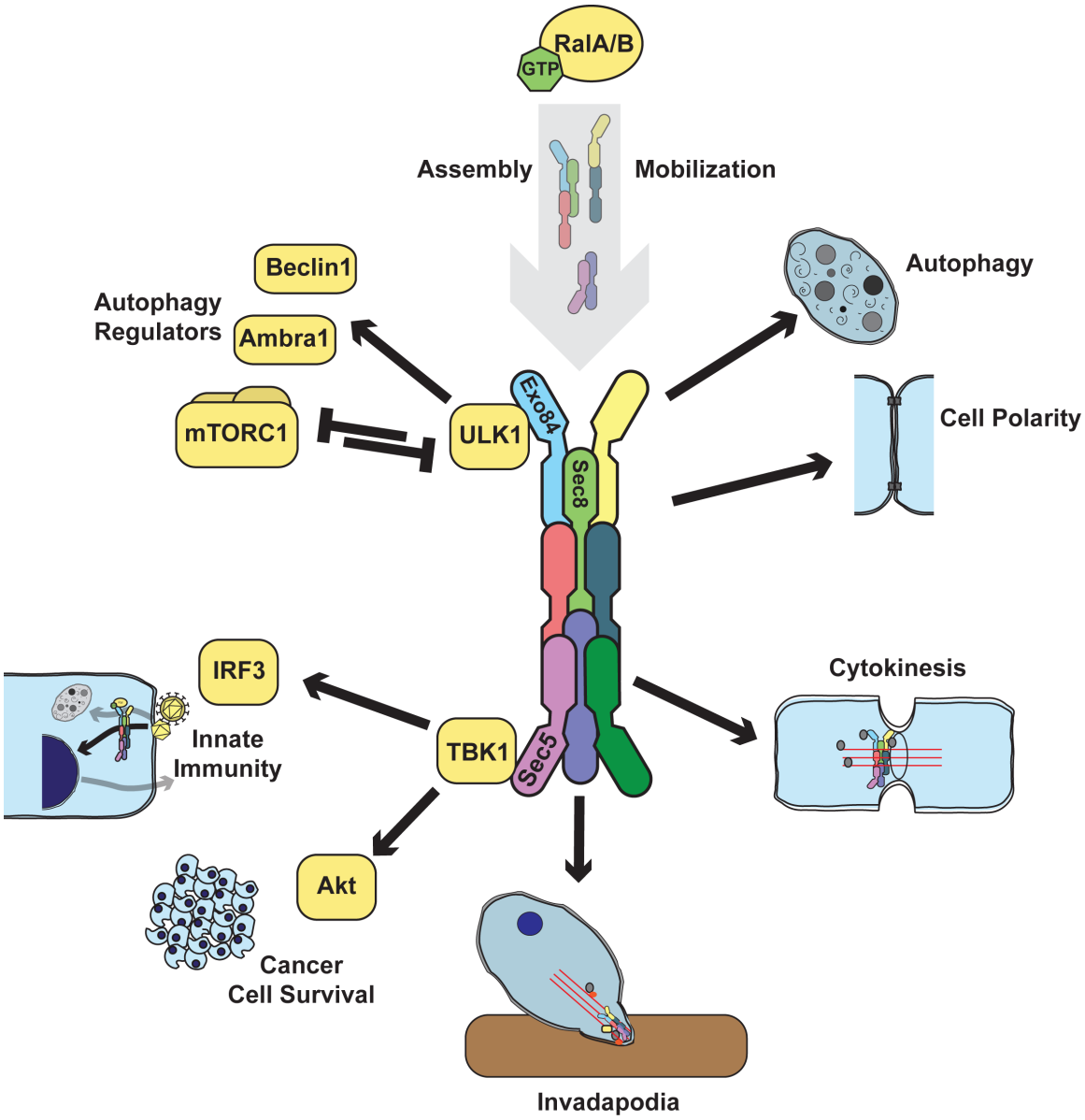

Figure 1: Summary of exocyst regulation.

CHAPTER TWO

TBK1 Directly Engages Akt/PKB Survival Signaling to Support Oncogenic Transformation

Introduction

The atypical IκB kinase family member TBK1 (TANK-binding kinase 1) has been defined as a principle hub in cell regulatory networks responsive to inflammatory cytokines and pathogen surveillance receptors[24-26]. Together with its homologue IKKε, TBK1 marshals the IRF3 and IRF7 transcription factors to induce type I interferon expression and activation of other components of the immediate early host defense response. As such, TBK1 and IKKε are required elements of innate immune signaling in most epithelia and stromal cell types[25-28].

In cancer cells, pathological TBK1 activation supports oncogenic transformation by suppressing a programmed cell death response to oncogene activation[29]. TBK1 kinase activity is engaged by Ras through the RalGEF-RalB-Sec5 effector pathway, is elevated in transformed cells, and is required for their survival in culture[22,30]. Systematic RNAi screens of diverse tumor-derived cell lines confirmed that a codependent relationship between oncogenic Ras and the RalB/Sec5/TBK1 pathway is conserved in a variety of disease settings[31].

While IRF3 is a direct TBK1 substrate that clearly accounts for much of the role of TBK1 in support of innate immune signaling[24,32], TBK1 substrates that mediate cancer cell

survival are ill defined. Studies employing IRF3$^{-/-}$ MEFs or RNAi-mediated IRF3 depletion from cancer cell lines indicated this canonical TBK1 substrate is not an obligate component of TBK1-driven cell survival signaling[22,31], but may be important for pro-angiogenic signaling[30]. Using TBK1$^{-/-}$ cells to parse TBK1-dependent Ras-induced regulatory events, we found TBK1 is required for oncogenic Ras activation of AKT and concomitant mTOR activation and GSK3β suppression. Insulin-induced AKT activation is intact in TBK1$^{-/-}$ MEFs, however TLR4, TLR3, EGFR and glucose-induced AKT activation is impaired. In human epithelial cells, these TBK1-dependent signals recruit endogenous TBK1 to the exocyst where it activates AKT. Furthermore, TBK1 depletion impairs both mitogen and oncogene activation of AKT in human cells. We find that TBK1 directly interacts with AKT and is sufficient to drive both activation loop, T308, and hydrophobic motif, S473, phosphorylation in cells and within an *in vitro* biochemical reconstitution system. Consistent with these observations, TBK1 activation of AKT in cells can occur in the absence of the canonical AKT-T308 and AKT-S473 kinases, PDK1 and mTORC2. Loss of TBK1 is toxic to most, but not all oncogenic Ras expressing tumor lines *in vitro* and *in vivo*, and this toxicity can be rescued by expression of mutationally activated AKT. A novel chemical inhibitor of TBK1 kinase activity, with potency in the nanomolar range, was isolated from a 250,000 compound screen. This 6-aminopyrazolopyrimidine derivative is selectively toxic to TBK1-dependent cancer cell lines. Furthermore, the compound can inhibit AKT activation in these cells without affecting the canonical AKT activators PDK1 or mTOR. Thus AKT likely represents a bona fide TBK1 substrate protein that mediates TBK1-dependent signaling in normal and

tumorigenic contexts. The phenotypic concordance of TBK1 homozygous deletion, RNAi-mediated TBK1 depletion and pharmacological inhibition of TBK1 kinase activity reveals TBK1 as a targetable link supporting context-selective mobilization of the AKT regulatory network.

Results

Previous observations that TBK1$^{-/-}$ MEFs fail to support oncogenic Ras-induced transformation, at least in part due to survival defects[22], prompted us to examine survival pathway activation in this setting. As expected, lentiviral-mediated transient expression of K-RasG12V in wild-type mouse embryo fibroblasts resulted in excess AKT activation as indicated by accumulation of activation site phosphorylation[5-7,33-35]. In contrast, despite equivalent K-RasG12V expression, TBK1$^{-/-}$ MEFs did not support AKT activation by oncogenic Ras (Figure 1A). Selection of stable populations of wild-type and TBK1$^{-/-}$ MEFs, with similar amounts of K-RasG12V expression, showed marked differences in the formation of growth transformed foci, accumulation of active AKT, and concomitant engagement of the mTOR pathway (Figure 1B). Transient siRNA-mediated TBK1 depletion in human osteosarcoma cells and telomerase-immortalized airway epithelial cells with multiple independent siRNAs resulted in reduced accumulation of active AKT as compared to controls (Figure 1C). Collectively, these observations suggest TBK1 supports AKT pathway activation in multiple regulatory contexts.

We have previously defined the heterooctameric Sec6/8 a.k.a. exocyst complex as a hub for Ras activation of TBK1 via the RalB effector pathway[8,21,22,36]. A protein/protein interaction map, generated by saturating genome-wide yeast two-hybrid screens of each human exocyst subunit against a human placenta library, identified AKT1 and AKT2 interactions with two distinct exocyst subunits- Exo70 and Sec3 (Figure 1D). The association of AKT with the exocyst was validated by expression co-IP (Figure 1E) as well as recovery of native exocyst components from endogenous AKT immunoprecipitates (see Figure 3D). The functional relevance of this association is suggested by impaired accumulation of active AKT upon Sec3 depletion from U2OS cells (Figure 1C). Immunoprecipitates of native exocyst complexes from multiple cell types selectively coprecipitated endogenous TBK1 versus the closely related family member, IKKε, further implicating TBK1 and the exocyst in AKT activation (Figure 1F).

To assess the context-selective contribution of TBK1 to AKT activation, we evaluated the responsiveness of $TBK1^{-/-}$ cells to a variety of germane AKT pathway agonists (Figure 2). We found that AKT was equivalently responsive to insulin in both wild-type and $TBK1^{-/-}$ MEFs, indicating that insulin-induced AKT activation is TBK1-independent (Figure 2A). In contrast, AKT-responsiveness to EGF or glucose was impaired in the absence of TBK1 (Figure 2B,D). In addition, AKT-responsiveness to innate immune pathway activation by either Sendai virus infection or LPS exposure was severely blunted in the absence of TBK1 as compared to wild-type MEFs (Figure 2F). Complementation of $TBK1^{-/-}$ MEFs using human wild-type TBK1 rescued AKT activation by EGF and

glucose (Figure 2C,E). We did not observe activation of IFNβ expression, a canonical TBK1 effector pathway, in response to EGF or glucose reexposure in these cells (Figure 2G). However, TBK1$^{-/-}$ MEFs were refractory to EGF-induced proliferation (Figure 2H) and sensitized to apoptosis upon serum or glucose withdrawal (Figure 2I). Together, these observations reveal a stimulus-selective contribution of TBK1 to AKT pathway activation.

Examination of full-length and truncated proteins indicated that TBK1 and AKT can be reciprocally isolated in either TBK1 or AKT immunoprecipitates (Figure 3A) and that the association in cells is likely mediated through their respective kinase domains (Figure 3B,C). To examine native TBK1/AKT complex assembly, we tested the capacity of endogenous AKT to coimmunoprecipitate endogenous TBK1 in response to glucose exposure or innate immune pathway activation- two settings requiring TBK1 for AKT activation as indicated by observations in TBK1$^{-/-}$ MEFs (Figure 2). In glucose starved cells, the exocyst but not TBK1 coimmunoprecipitated with AKT. However, glucose stimulation recruited TBK1 to AKT complexes in all 4 human cell lines tested (Figure 3D). Sorbitol exposure was used as an osmolarity control (Figure 3D, middle top panel). These observations indicate that a population of AKT is constitutively associated with the exocyst, while TBK1 is recruited into the complex in a stimulus-dependent manner. Similarly, Sendai virus infection or LPS exposure drove assembly of native TBK1/AKT complexes (Figure 3E).

Both wild-type and kinase-dead TBK1 associated with AKT, however, only wild-type TBK1 immunoprecipitates contained active AKT, as indicated by serine 473 phosphorylation and *in vitro* kinase activity using a GSK3α/β fusion peptide as substrate (Figure 4A). Remarkably, TBK1 expression was sufficient to drive AKT activation in the face of pharmacological inactivation of the PI3K family (Figure 4B). Moreover, TBK1 induced AKT activation loop (T308) and hydrophobic motif (S473) phosphorylation in cells in the absence of PDK1 (Figure 4C,D) or the mTORC2 subunits Sin1 (Figure 4E) or Rictor (Figure 4F). These observations indicate that TBK1 is sufficient to induce AKT activation independently of the canonical PDK1/mTORC2 collaboration[9,34,37-42].

In the presence of ATP and Mg^{++}, purified recombinant TBK1 was sufficient to drive phosphorylation of both T308 and S473 on otherwise inactive recombinant AKT1 *in vitro* (Figure 4G). Moreover, this correlated with a 100-fold increase in AKT1 specific activity as detected using a GSK3α/β–derived peptide substrate (Figure 4G), and with significant accumulation of phosphorylation of AKT autosubstrate sites (Figure 4H)[10,43]. Endogenous TBK1 immunoprecipitated from MEFs also directly phosphorylated recombinant AKT (Figure 4I). Consistent with a role for TBK1 in EGF-induced AKT activation in MEFs (Figure 2B) TBK1 kinase activity was enhanced by EGF stimulation (Figure 4I). Similar observations using kinase-dead and wild-type proteins immunopurified from HEK293T cells indicated that TBK1-induced phosphorylation of AKT-T308 and AKT-S473 was dependent upon an intact TBK1 kinase domain, and

independent of AKT kinase activity (Figure 4J). As expected, TBK1 induction of AKT autosubstrate site phosphorylation only occurred with catalytically intact AKT (Figure 4J). Thus, to our knowledge, TBK1 is the first kinase identified as sufficient to directly activate AKT. The disease significance of this non-canonical regulatory arm is suggested by the observation that, in the absence of PDK1, oncogenic Ras signaling to AKT is only partially blunted and the responsiveness of AKT effectors is unaffected (Figure 4K).

To examine the consequence of TBK1 on tumorigenicity, we first depleted TBK1 using lentiviral transduction of shRNAs in Mia-Paca2 cells, a pancreas cancer cell line with the K-RasG12C mutation[11,44]. Two of three hairpins resulted in detectable TBK1 depletion by 2 days post transduction with concomitant reduction in AKT activation (Figure 5A). By 6 days post transduction, the viability of TBK1 depleted cells was severely compromised (Figure 5B), but could be rescued by expression of an artificially activated myristoylated AKT fusion protein (Figure 5C). To examine if the cell death observed in cultured cells was recapitulated in an orthotopic setting, Mia-Paca-2 cells were surgically implanted beneath the capsule of the tail of the pancreas of immune-compromised mice two days post transduction with shRNA expressing lentiviral constructs. Two independent TBK1 shRNAs impaired primary tumor initiation (Figure 5D) and progression (Figure 5E) as compared to controls. Equivalent experiments were also performed in MDA-MB-231 cells, a triple negative breast cancer derived cell line with activating mutations in both K-Ras and B-Raf[12,44]. MDA-MB-231 cells, transduced with shRNA-expressing lentivirus, were implanted into the mammary fat pad of immune

compromised mice and tumor growth was followed (Figure 5F). By 45 days post-implantation, control samples had progressed substantially (Figure 5G) and metastasized to other organs (Figure 5H). In contrast, TBK1-depleted samples progressed very poorly and failed to metastasize (Figure 5F,G,H). These observations indicate that TBK1 is required to support AKT activation in cancer cells, and is required for primary tumor initiation and progression, at least in the context of two different orthotopic xenograft models.

To discriminate the consequence of TBK1 depletion from inhibition of TBK1 kinase activity, we wished to employ small molecule TBK1 inhibitors for pharmacological interrogation of the TBK1/AKT regulatory relationship in normal and cancer cells. The currently available compound, BX795[13,45,46], has significant activity against both TBK1 and PDK1, which limits its application to these studies [14,47]. Therefore, we isolated additional chemical TBK1 inhibitors from a biochemical screen of ~250,000 small molecules. A 6-aminopyrazolopyrimidine derivative (Compound II, Figure 6A) was identified as a lead compound with an IC_{50} of 13 nM against TBK1 and 59 nM against the TBK1 homolog IKKε, but with 100- to 1000-fold less activity against other tested protein kinases including PDK1, PI3K family members and mTOR (Figure 6B). Consistent with inhibition of TBK1-dependent signaling, compound II inhibited LPS-induced expression of IFNβ (IC_{50} =62nM), and the IFNβ target genes IP10 (IC_{50} =78nM) and Mx1 (IC_{50} =20nM) (Figure 6C). Consistent with selective activity on canonical TBK1 pathway activation[15,16,48,49], Compound II effectively blocked TLR3-

dependent IRF3 nuclear translocation in cells with an IC_{50} under 100 nM, but did not impair TNFR1-dependent p65 NFκB nuclear translocation with doses as high as 20 μM (Figure 6D). This later response has been defined as TBK1-independent [17,18,22,48,50]. Concordant with our observations in $TBK1^{-/-}$ MEFs, a 30-minute pretreatment of wild-type MEFs with Compound II impaired AKT activation by glucose (Figure 6E). Similarly, a 30-minute incubation of the TBK1-sensitive cell line HCC44 with doses of Compound II as low as 500 nM was sufficient to blunt baseline AKT activity (Figure 6F). Notably, Compound II had no activity against the canonical AKT kinases PDK1 and mTOR *in vitro* (Figure 6B), indicating the defective AKT response is likely a consequence of impaired TBK1 activity. Concordant with mTORC2-independent activation of AKT by TBK1, the AKT response to host defense signaling in $Sin1^{-/-}$ and $Rictor^{-/-}$ cells was blocked by Compound II (Figure 6G). Concordant with the consequence of siRNA and shRNA-mediated TBK1 depletion, a 24-hour exposure to Compound II inhibited AKT pathway activation and survival in multiple cancer cell lines at doses close to those affecting IRF-3 nuclear localization (Figure 6H). Importantly, the extent of AKT inhibition was equivalent or better than that observed with 40 μM of the PI3K inhibitor LY294002 (Figure 6H).

We next examined if cancer cell lines selectively sensitive to shRNA-mediated TBK1 depletion were also selectively sensitive to Compound II. First, to assess the incidence of TBK1-sensitivity across diverse oncogenotypes within a discrete disease setting, we employed a panel non-small cell lung cancer (NSCLC) derived cells lines for which the

oncogenic Ras status had been defined. We collected 15 lines, 10 of which express oncogenic K-Ras, and examined the consequence of TBK1 depletion on cell viability using two independent TBK1 shRNAs. We found that TBK1 depletion was toxic to approximately 50% of this cohort (Figure 7A). Of note, H1993 (TBK1-sensitive) and H2073 (TBK1-resistant) are derived from a lymph node metastasis and the primary tumor, respectively, from the same patient. Although many lines with oncogenic Ras mutations were in the TBK1-dependent class (6 of 10), the presence of this oncogene is not solely sufficient to specify TBK1-sensitivity. A recent study examining the relative addiction of NSCLC cell lines to oncogenic Ras expression indicated that lines with epithelial characteristics, including elevated E-cadherin expression, were selectively dependent on the continued expression of oncogenic Ras[6,51]. However, this relationship also failed to specify TBK1-sensitivity (Figure 7A, lower panels), suggesting additional key biological determinants driving TBK1 addiction remain to be discovered. A549 (TBK1-dependent) and H441 (TBK1-independent) were exposed to Compound II for 96 hours across a nanomolar to micromolar dose range, with cell viability as the endpoint assay. Importantly A549 cells (IC_{50} ~ 0.4 micromolar) were acutely responsive to compound II concentrations at least 10 fold lower than those required for significant toxicity in H441 cells (IC_{50} ~ 4.2 micromolar) (Figure 7B). In addition, TBK1-dependent lines were selectively sensitive to induction of apoptosis upon a 24-hour exposure to 2 micromolar Compound II as compared to TBK1-independent lines (Figure 7C). Compound II exposure strongly suppressed accumulation of active AKT in all TBK1-sensitive NSCLC lines tested (H358, H1993, and HCC44). In contrast the TBK1-

independent cell lines H2073 and H441 maintained chronic AKT activation in the presence of Compound II (Figure 7D). Calu1, which displays intermediate sensitivity to TBK1 depletion (Figure 7A), also displayed intermediate sensitivity to Compound II-dependent inhibition of AKT activation (Figure 7D). These concordant observations between RNAi-mediated TBK1 depletion and small molecule mediated inhibition of TBK1 activity indicate that TBK1 represents an important direct regulatory input to AKT survival signaling.

Discussion

Beyond its canonical occupation as a core component of innate immune and inflammatory cytokine signaling, TBK1 has attracted attention as a potential therapeutic target in cancer given its selective support of cancer cell viability[19,22,31]. Here, we have identified the survival signaling kinase AKT/PKB as a direct TBK1 effector. Upon genetic ablation, RNAi-mediated depletion, or pharmacological inactivation of TBK1, AKT activity is diminished and cancer cell viability is impaired. The mechanistic basis of TBK1 support of AKT activation is direct stimulation of AKT catalytic activity as a consequence of TBK1-induced phosphorylation of both the T308 activation loop residue and the S473 hydrophobic domain residue. TBK1 expression is required to support pathological oncogene-dependent AKT signaling, and is required to fully engage AKT in response to EGF, glucose, and host defense signaling. Insulin responsiveness, on the other hand, is TBK1-independent.

The PDK1 kinase and mTORC2 complex have been defined as key proximal determinants of AKT activation. mTORC2 directly phosphorylates AKT-S473, which in turn promotes direct phosphorylation of T308 by PDK1 in the presence of appropriate collateral accumulation of the PI3K product phosphatidylinositol-3,4,5-trisphosphate (PIP_3) [20,34,37,38,41]. This collaborative action is required for AKT activation by insulin[7,52], though the mechanism of mTORC2 activation in this context is currently unknown[5,34]. Our observations suggest that the contribution of TBK1 to AKT activation is non-redundant to the PDK1/mTORC2 pathway. For example, the PDK1/mTORC2 pathway is apparently intact in $TBK1^{-/-}$ MEFs given the wild-type responsiveness of AKT to insulin in these cells. However, the defective AKT responsiveness to EGF, glucose, or innate immune signaling indicates that PDK1/mTORC2 are not sufficient to engage AKT downstream of all germane regulatory inputs. Most importantly, TBK1 retains the capacity to activate AKT in cells where PDK1 or the mTORC2 subunits Sin1 or Rictor have been homozygously deleted.

We find that a subpopulation of AKT in cells is associated with the Sec6/8 a.k.a. exocyst complex. This heterooctameric protein complex was originally identified through its role in the regulated targeting and tethering of selected secretory vesicles to specialized dynamic plasma membrane domains[21,53,54]. Subsequently, it was discovered that the exocyst plays a direct role in host defense signaling by marshaling TBK1 and STING (stimulator of interferon genes) in response to cellular detection of viral replication intermediates[22,29,55,56]. The recruitment of TBK1 to the exocyst in response to AKT

pathway agonists that are TBK1 dependent, together with the observation that exocyst integrity supports AKT activation, suggests that this protein complex may represent an architecturally discrete signaling platform. Distinct regulatory inputs to AKT, which can be separately or simultaneously operative, could support compartmentalization of AKT activity within a cell, perhaps as a mechanism to specify the cadre of client substrates engaged by AKT in response to diverse agonists[23,40,57].

Chemical inhibitors of TBK1 will be valuable in further clarifying the role of TBK1 in AKT survival signaling, and defining the therapeutic value of this kinase target. As a tool compound, Compound II was found to be effective in the low nanomolar range in vitro, cell permeable, and a potent and selective TBK1 inhibitor in cells. Importantly, Compound II exposure impaired accumulation of active AKT, and displayed selective toxicity in TBK1-dependent cancer cell lines. The concordant observations with Compound II exposure and TBK1 depletion strongly suggest that the phenotypes reported here are most likely a consequence of TBK1 catalytic activity as opposed to activity-independent consequences of TBK1 depletion. This indicates that TBK1 support of pathological AKT activation can likely be pharmacologically targeted in disease. In conclusion, our observations define AKT as a direct TBK1 effector and reveal a non-canonical context-selective regulatory mechanism for mobilization of AKT signaling.

ACKNOWLEDGEMENTS

We are grateful to Zhijian James Chen, Xuetao Cao, Philip N. Tsichlis, Charles Yeaman, William Hahn, Keqiang Ye, and Shu-Chan Hsu, Bing Su, Dos Sarbassov, Mark

Magnuson, David Sabatini and Bert Vogelstein for many of the reagents used in these studies. We thank Melanie H. Cobb, Philip N. Tsichlis, Lawrence Lum, and members of our laboratory for invaluable advice and discussion. This work was supported by the National Institutes of Health (CA71443 and CA129451) and the Robert Welch Foundation (I-1414).

Materials and Methods

Cell culture and transfection. $TBK1^{+/+}$ and $TBK1^{-/-}$ MEFs, Mia-Paca2, U2OS, Panc-1, HEK293T, HBEC, HeLa and MCF7 cells were cultured as previously described[22], and $Sin^{-/-}$ MEFs, kindly provided by Dr. Bing Su (Yale University), $Rictor^{-/-}$ MEFs, kindly provided by Drs. Mark Magnuson (Vanderbilt University School of Medicine), Dos Sarbassov (The University of Texas MD Anderson Cancer Center) and David Sabatini (Massachusetts Institute of Technology), and MDA-MB-231 cells were cultured in DMEM supplemented with 10% fetal bovine serum (Atlanta Biologicals), 100 U/mL penicillin and 100 μg/mL streptomycin (Invitrogen). Wild-type and $PDPK1^{-/-}$ HCT116 and DLD1 cells were kindly provided by Dr. Bert Vogelstein (Johns Hopkins University) and cultured as described[58]. Lung cancer cell lines A549, Calu1, Calu6, H1155, H1819, H1993, H2073, HCC366, H358, H441, H460, H727, HCC827, HCC44 and Sklu1 cells were cultured in RPMI supplemented with 5% fetal bovine serum (Atlanta Biologicals), 100 U/mL penicillin and 100 μg/mL streptomycin (Invitrogen). For siRNA transfection, U2OS and HBEC cells were transfected with siRNA using DharmaFECT 1 (Dharmacon)

as described[59]. Sin$^{-/-}$ MEFs, Rictor$^{-/-}$ MEFs, PDK1$^{-/-}$ HCT116 and DLD1 cells were transfected with ExGen 500 (Fermentas) according to manufacturer's instructions. HeLa cells were transfected with LF2000 (Invitrogen).

Plasmids, reagents and antibodies. The mammalian expression plasmids pCDNA-FLAG-TBK1 (WT) and (K38M) were generously provided by Dr. James Chen (UT Southwestern Medical Center), and are as described[25-28,60]. To construct the pRK5-Myc-FLAG-TBK1 (WT) and (K38M) mammalian expression plasmids, TBK1 coding sequences were excised from pCDNA-FLAG-TBK1 (WT) and (K38M) and subcloned into the *BamHI* and *XbaI* sites of pRK5-Myc. HA-TBK1 (WT) and HA-TBK1 (NT) expression vectors were generously provided by Dr. Xuetao Cao (Second Military Medical University, Shanghai, China)[29,61]. Wild-type and kinase-dead HA-AKT1, and myristoylated-HA-AKT1 were generously provided by Dr. Philip N. Tsichlis (Tufts Medical Center)[22,30,62]. GST-AKT1 full-length and truncation mutants were generously provided by Dr. Keqiang Ye (Emory University School of Medicine) [31,63,64]. Lenti-virus shRNA expression constructs were generously provided by Dr. William Hahn (Harvard Medical School). Myc-Sec8, Sec3-GFP, and Exo70-GFP expression constructs were generously provided by Dr. Charles Yeaman (University of Iowa) [24,32,65]. Recombinant His-TBK1 (no. 14-628), and His-AKT1 (inactive, no. 14-279) were purchased from Upstate/Millipore Corp. AKT Kinase Assay kits (no. 9840) were purchased from Cell Signaling Technology. Glutathione (GSH)-Sepharose 4B (no. 17-0756-01) was purchased from GE Healthcare Amersham. Protein A/G (sc-2003) and anti-HA antibody

conjugated beads (sc-7392ac) were purchased from Santa Cruz. Anti-FLAG antibody conjugated beads (A2220), 3xFLAG peptide (F4799) and LY294002 (L9908) were purchased from Sigma. HA peptide (RP11735) was purchased from GenScript. Anti-Sec8 mouse monoclonal antibodies were kindly provided by Dr. Charles Yeaman (University of Iowa) [22,31,65] and anti-Exo70 mouse monoclonal antibodies were generously provided from Dr. Shu-Chan Hsu (Rutgers University)[30,66]. Additional antibodies were purchased from Sigma (anti-Actin, A1978), BioChain (anti-IKKε, Z5020108), Santa Cruz Technology (anti-K-Ras, sc-30; anti-ERK1/2, sc-93; anti-Myc, sc-40; anti-HA, sc-805; anti-IRF3, sc-9082), Cell Signaling Technology (anti-AKT1, 2967; anti-AKT-pS473, 4060; anti-AKT-pT308, 2965; anti-phospho-(Ser/Thr) AKT substrate, 9611; S6K, 9202; S6K-pT389, 9234 and 9206; S6, 2217; S6-pS235/236, 4858; TBK1, 3504; TSC2, 3635; TSC2-pT1462, 3611; Cleaved-PARP, 9541;), Upstate/Millipore Corp. (anti-TBK1, 04-856; anti-AKT1, 05-796) and Imgenex Corp. (anti-TBK1, IMG-139A).

Lentiviral transduction. Lentiviral-based expression constructs were packaged by cotransfection of HEK293FT cells with VSV-G and Δ-8.9 plasmids. Growth media was replaced with Opti-MEM 24 hours post transfection, and incubated a further 24 hours prior to viral particle collection. $TBK1^{+/+}$ and $TBK1^{-/-}$ MEFs were plated at a density of $4x10^4$ cells/well into 6-well plates. Twenty-four hours later, cells were infected with lentiviral particles and polybrene (10 μg/ml). $PDPK1^{+/+}$ and $PDPK1^{-/-}$ DLD1 cells were plated at a density of $1.25x10^5$ cells/well into 6-well plates. Twenty-four hours later,

cells were infected with lentiviral particles and polybrene (10 μg/ml). Mia-Paca2 and MDA-MB-231 cells were seeded at $1x10^5$ cells/well in 6-well plates. Twenty-four hours later, cells were infected with 1ml of lenti-viral particles containing indicated shRNAs for 2 hours, and then virus-containing medium (Opti-MEM) was replaced with 2 ml of normal medium. All NSCLC cell lines were seeded at $5x10^3$ cells/well into 96-well microtiter plates in triplicate and incubated overnight. Twenty-four hours later cells were infected with 90 μl of lenti-viral particles in Opti-MEM and polybrene (10 μg/ml) for 2 hours followed by a medium exchange with RPMI containing 5% FBS. On day 3 post-infection, cells were given fresh medium. On day 6, cells were equilibrated at r.t. for 30 min and then CellTiter-Glo reagent (15μl) was added to each well. Following 10 min incubation, samples were analyzed using an Envision plate reader.

Immunoprecipitation and affinity purification. Whole cell extracts were prepared in non-denaturing IP buffer (20 mM Tris HCl [pH 7.5], 10 mM $MgCl_2$, 2 mM EGTA, 10% Glycerol, 137 mM NaCl, 1% Triton X-100 (vol/vol), 0.5% Na Deoxycholate, 1 mM DTT, phosphatase and protease inhibitors [Roche]) were incubated with anti-AKT1 mouse monoclonal antibody (Cell Signaling) and 30 μl Protein A/G beads (Santa Cruz) overnight at 4^oC. Immunoprecipitates were washed three times in (20 mM Tris HCl [pH 7.5], 10 mM $MgCl_2$, 2 mM EGTA, 10% Glycerol, 137 mM NaCl, 1% Triton X-100 (vol/vol), 0.5% Na Deoxycholate, 1 mM DTT, and 1 mM PMSF) then boiled in standard SDS sample buffer. Samples were separated by SDS-PAGE followed by immunoblot analysis. Co-immunoprecipitation of overexpressed proteins from HEK293T cell lysates

was performed with 30 µl of anti-HA agarose beads (25% slurry) or anti-FLAG M2 beads (50% slurry). For mapping TBK1-interacting domain on AKT, a variety of GST-tagged AKT deletion mutants and Myc-FLAG-tagged TBK1 were expressed in HEK293T cells. Two-day post-transfection, cells were lysed in IP buffer, and then cell lysates were incubated with 30 µl GSH-Sepharose beads for 3 hours. After three washes with wash buffer, beads were boiled for 5 min in SDS sample buffer, and subjected to SDS-PAGE and immunobloting analysis. For mapping TBK1/AKT interaction domains, GST-tagged AKT kinase-domain and either HA-tagged full-length or N-terminal TBK1 were expressed in HEK293T cells. Two-day post-transfection, cells were lysed in IP buffer, and then cell lysates were incubated with 30 µl GSH-Sepharose beads for 3 hours. After three washes with wash buffer, beads were boiled for 5 min in SDS sample buffer, and subjected to SDS-PAGE and immunoblot analysis.

Immunofluorescence. For quantitative detection of endogenous IRF3 nuclear localization in response to Poly I:C, 15,000 HeLa cells/well were seeded in 96-well plates in medium containing 10% FBS. Compound (10 doses, starting from 20 µM, then 1:5 serially diluted) and 5 µg/ml of poly I:C (Sigma, P-9582) mixed with 3 µl/ml of LF 2000 were added and cells were incubated for 2 hrs. Cells were then fixed with 3.7% formaldehyde for 15 min., permeabilized with 0.5% Triton-X for 15 min., then stained with anti-IRF3 antibody for an hour followed by Alexa488 secondary antibody and Hoechst nuclear staining for another hour. Intensity of IRF3 in nucleus vs. IRF3 in cytoplasm was measured using Cellomics ArrayScan and analyzed using vHCS View and

GraphPad Prism. For quantitative detection of endogenous p65 nuclear translocation in response to TNF, HeLa cells were handled as described above except that cells were pretreated with serially diluted compound for 10 minutes prior to exposure to 10 ng/ml TNFα for 10 minutes. p65 was detected with a rabbit polyclonal anti-p65 and the Alexa488 secondary antibody and nuclear accumulation was quantitated as above. For Annexin V labeling, cells were harvested with trypsin, washed two times in PBS, resuspended in 100 µl Annexin V binding buffer (10 mM HEPES pH 7.4, 140 mM NaCl, 2.5 mM $CaCl_2$) and incubated with 5 µl FITC Annexin V (BD Pharmingen, 51-65874X) at r.t. for 15 min. Samples were then subjected to FACS Calibur (BD Biosciences) and analyzed using CellQuest software (BD Biosciences). For BrdU incorporation assays, WT and $TBK1^{-/-}$ MEFs were seeded onto cover slips overnight and then either maintained in the presence or absence of serum for 44 hr. Cells were treated with BrdU (10 µM; Sigma, B9285) together with either carrier, EGF (100ng/ml) or FBS (10%) simultaneously. After 4 hours, cells were washed with PBS, fixed by 3.7% Formaldehyde for overnight at 4 ^{0}C, and then permeabilized with cold acetone for 5 min. Following PBS washes, cells were treated with 2N HCl for 10min at R.T. then washed again. Cover slips were blocked with PBTA (PBS, 1% Tween 20, and 1% BSA) for 30 min at R.T., and then incubated with anti-BrdU antibody (1:20; Invitrogen, A21303) for 1 hr. Following extensive washing, cells were stained with DAPI and mounted. BrdU positive cells were counted as percentage relative to total nuclei (DAPI stain). For measuring cell death, WT and $TBK1^{-/-}$ MEFs were seeded onto cover slips overnight. Cells were either maintained in the presence of serum, serum starved, or glucose deprived. After 24hr cells were fixed

and stained with DAPI. Pyknotic cells were counted as percentage relative to total nuclei (DAPI stain).

AKT affinity purification. HA-AKT wild-type or kinase-dead was expressed in HEK293T cells. Two days post-transfection, cells were incubated overnight in DMEM without serum, and then lysed in IP buffer. HA-AKT proteins were purified with anti-HA beads, and washed extensively (20 mM Tris-HCl, and 1 M NaCl; pH 7.5). HA-AKT proteins were then released with elution buffer (1 mg/ml HA peptide, 20 mM Tris-HCl, 0.1 M NaCl, and 0.1 mM EDTA; pH 7.5). The concentrations and purity of HA-AKT wild-type and kinase-dead proteins were determined by Coomassie blue staining.

***In Vitro* protein kinase activity assays.** For *in vitro* kinase assays with purified recombinant proteins, 20 ng of His-tagged TBK1 and 100 ng of His-tagged AKT were mixed as indicated in kinase buffer (25 mM Tris HCl [pH 7.5], 10 mM $MgCl_2$, 5 mM β-Glycerophosphate, 2 mM DTT, and 0.1 mM Na_3VO_4) containing 200 μM ATP at 30°C. After 30 min. incubation, 1 μg of GST-GSK3α/β AKT substrate peptides (CGPKGPGRRRTSSFAEG) and 200 μM ATP were added and kinase reactions were performed for additional 30 min at 30°C. Phosphorylation of the AKT substrate sites on the GSK3α/β peptide was detected using the phospho-GSK-3α/β (Ser21/9) antibody (Cell Signaling). For IP kinase assays, HA-AKT and Myc-FLAG-TBK1 were expressed in HEK293T cells. Cells were lysed in IP buffer and immunoprecipitation was performed with anti-HA beads or anti-FLAG M2 beads, respectively. Following

extensive washing with IP buffer containing 0.1% SDS, beads were suspended in kinase buffer (25 mM Tris HCl [pH 7.5], 10 mM $MgCl_2$, 5 mM β-Glycerophosphate, 2 mM DTT, and 0.1 mM Na_3VO_4), and reactions were performed at 30^oC in 50 µl kinase buffer containing 100 µg/ml 3xFLAG peptides, 200 µM ATP, and either purified HA-AKT wild-type or kinase-dead as indicated. After 30 minutes, reaction mixtures were boiled for 5 min in SDS sample buffer, and subjected to SDS-PAGE and immunoblot analysis. For measuring native TBK1 kinase activity, WT MEFs were starved overnight and treated as indicated. IP kinase assays were then performed by using anti-TBK1 antibody (Cell Signaling) and His-tagged AKT as substrate following above-mentioned procedure.

Chemical compound screen. A library of 256,953 kinase inhibitor-biased compounds were screened against full-length TBK1 (Invitrogen) using an HTRF assay from the CisBio KinEase system. Compounds were screened at single dose of 25 µM in the presence of 6 nM TBK1, 1 µM STK3, and 10 µM ATP (2xKm) using the HTRF KinEASE S3 kit. 917 compounds which inhibited >40% of TBK1 activity were selected for single-point reconfirmation. Dose-response studies were performed on 818 confirmed hits, and compounds with IC_{50} < 1 µM were selected for follow-up studies. Compound II was found to be a potent inhibitor of TBK1 and IKKε in both biochemical and cell-based assays. In-house kinase cross-screening revealed a reasonable selectivity profile in that Compound II does not inhibit IKK α/β kinases and known kinase mediators of the PI3K-AKT-mTOR pathway.

Yeast two-hybrid screens. The coding sequences for amino acids 1-222 of human AKT1 (GenBank gi:6224101) and amino acids 111 – 222 of human AKT2 (GenBank gi: 6715585) were cloned into pB6 as a C-terminal fusion to Gal4 DNA Binding Domain. The constructs were used as baits to screen at saturation a highly complex, random-primed human placenta cDNA library constructed in pP6. pB6 and pP6 derive from the original pAS2ΔΔ [22,67](Fromont-Racine et al., 1997) and pGADGH [68] plasmids, respectively. 60 million clones (6-fold the complexity of the library) were screened with each bait using a mating approach with Y187 (matα) and CG1945 (mata) yeast strains as previously described[67]. Positive colonies were selected on a medium lacking tryptophan, leucine and histidine. The prey fragments of the positive clones were amplified by PCR and sequenced at their 5' and 3' junctions. The resulting sequences were used to identify the corresponding interacting proteins in the GenBank database (NCBI) using a fully automated procedure. A confidence score (PBS, for Predicted Biological Score) was attributed to each interaction as previously described[69]. The PBS relies on two different levels of analysis. First, a local score takes into account the redundancy and independency of prey fragments, as well as the distribution of reading frames and stop codons in overlapping fragments. Second, a global score takes into account the interactions found in all the screens performed at Hybrigenics using the same library. This global score represents the probability of an interaction being nonspecific. For practical use, the scores were divided into four categories, from A (highest confidence) to D (lowest confidence). A fifth category (E) specifically flags interactions involving highly connected prey domains previously found several times in screens performed on

libraries derived from the same organism. Finally, several of these highly connected domains have been confirmed as false-positives of the technique and are now tagged as F. The PBS scores have been shown to positively correlate with the biological significance of interactions[70,71].

Orthotopic xenograft tumor models. 6-8 week old female NOD/SCID mice were purchased from an on-campus supplier. Animals were housed in a pathogen free facility and all animal studies were performed on a protocol approved by the IACUC at the University of Texas Southwestern Medical Center. For the orthotopic breast cancer model, SCID mice were anesthetized using inhaled isoflurane and 5 x 10^6 naïve or infected MDA-MB-231 cells were injected into the mammary fat pad (MFP) using previously described techniques[72]. Briefly, a small incision was made over the right axillary fat pad and the cells were injected in a volume of 50 µl using a 30-gauge needle. The incision was closed with a simple suture. Caliper measurements were performed twice weekly and tumor volume was calculated as D x d^2 x 0.52, where D is the long diameter and d is the perpendicular short diameter. Animals were sacrificed on post-injection day 48. At necropsy, tumor weights were calculated and lung metastases were evaluated by visual inspection. For the orthotopic pancreatic cancer model, animals were anesthetized using inhaled isoflurane. The abdominal wall and peritoneum were opened and the inferior pole of the spleen and tail of the pancreas were externalized through the wound. 1 x 10^6 naïve or infected Mia-Paca-2 cells in 50 µl PBS were injected into the tail of the pancreas using a 30g needle. The skin and abdominal

musculature were closed with a non-absorbable suture. Mice were monitored and weighed twice weekly. Animals were sacrificed at 7 weeks post-injection. At necropsy, liver, nodal, splenic, GI and peritoneal metastases were evaluated by visual inspection. Tumors weights were calculated in conjunction with residual pancreas[73].

Complementation assays. Mia-Paca2 cells were seeded at $2.5x10^3$ into 96-well format in triplicate and incubated overnight. Twenty-four hours later cells were transfected with constructs encoding either empty vector (EV) or constitutively-activated myristoylated-AKT (myr-AKT) by using ExGen 500. Forty-eight hours post-transfection, cells were infected with 90 µl of lentiviral particles containing indicated shRNAs for 2 hours, and then virus-containing medium (Opti-MEM) was replaced with 100 µl normal medium. On day 3 post-infection, cells were given fresh medium. On day 6, cells were equilibrated at r.t. for 30 min and then CellTiter-Glo reagent (15 µl) was added to each well. After 10 min incubation, samples were analyzed using an Envision plate reader.

Measurement of interferonβ production. Wild WT and $TBK1^{-/-}$ MEFs were seeded at $3x10^3$ into 96-well format in triplicate and incubated overnight. Cells were either maintained in the presence of serum, serum starved, or glucose deprived overnight, and then treated with Sendai viruses, EGF, or glucose respectively for 19 hours as indicated. Expression of interferonβ was measured using the mouse interferonβ ELISA (PBL Biomedical Laboratories).

Quantitative cytokine gene expression assays. Bone marrow derived macrophages were obtained by culturing C57/BL6 mice bone marrow cells in RPMI medium containing 10% FBS and 100ng/ml CSF-1 (Amgen Inc) for 6 days. To test the effect of TBK1 inhibitors on LPS induced gene expression, bone marrow derived macrophages were stimulated with 10ng/ml LPS (Sigma Aldrich) for 3 hours. mRNA was prepared using a standard mRNA extraction kit (Qiagen Inc). Real-time PCR was performed using the ABI PRISM 7900HT sequence detection system (PerkinElmer). Primers and probes were purchased from Applied Biosystems. Values were calculated based on standard curves generated for each gene. Expression levels of gene of interest were expressed relative to GAPDH.

Primers, siRNAs, and shRNAs. Synthetic siRNAs targeting TBK1 and Sec3 were obtained from Dharmacon. The followings are sense sequences of siRNA: Sequences of siTBK1-1 (5'-GACAGAAGUUGUGAUCACAdTdT-3') and siTBK1-2 (5'-CCUCUGAAUACCAUAGGAUdTdT-3') were previously described. siRNA pools targeting TBK1 (siGENOME) were a mixture of four independent siRNA containing the following sense sequences: D-003788-01 (5'-GAACGUAGAUUAGCUUAU-3'); D-003788-02 (5'-UGACAGAGAUUUACUAUCA-3'); D-003788-06 (5'-UAAAGUACAUCCACGUUAU-3'); D-003788-07 (5'-GGAUAUCGACAGCAGAUUA-3'). siRNA pools targeting Sec3 (siGENOME) were a mixture of four independent siRNA containing the following sense sequences: D-013312-01 (5'- 5'-GAAAUUAACUGGAUCUACU-3'-3'); D-013312-02 (5'-

GUAAAGUCAUUAAGGAGUA-3'); D-013312-03 (5'-GAAUGUAGCUCUUCGACCA-3'); D-013312-04 (5'-GAUUAUUUAUCCCGACUAU-3'). Lentiviral shRNAs expression constructs were based on the following hairpin sequences: pLKO.1-shTBK1-3 (Clone ID: TRCN0000003183: CCGGGTATTTGATGTGGTCGTGTAACTCGAGTTACACGACCACATCAAATACTTTTT); pLKO.1-shTBK1-4 (Clone ID: TRCN0000003184: CCGGCCAGGAAATATCATGCGTGTTCTCGAGAACACGCATGATATTTCCTGGTTTTT); pLKO.1-shTBK1-6 (Clone ID: TRCN0000003186: CCGGCGGGAACCTCTGAATACCATACTCGAGTATGGTATTCAGAGGTTCCCGTTTTT); pLKO.1-shGFP: GCCCGCAAGCTGACCCTGAAGTTCATTCAAGAGATGAACTTCAGGGTCAGCTTGCTTTTT)

Figure Legends

Figure 1. TBK1 and the exocyst support AKT activation.

(A) Wild-type (WT) and TBK1 homozygous null ($TBK1^{-/-}$) mouse embryonic fibroblasts (MEF) were infected with lentivirus encoding GFP or K-RasG12V[22]. Five days post-infection, whole cell lysates were prepared and relative accumulation of AKT-pS473, total K-Ras, TBK1, and AKT was assessed by immunoblot. (Approximate detected molecular size: K-Ras, 21KDa; TBK1, 84KDa; AKT, 60KDa; AKT-pS473, 60KDa; AKT-pT308, 60KDa)

(B) WT and TBK1$^{-/-}$ MEFs with equivalent stable expression of K-Ras G12V were seeded at low density and grown to confluence under standard culture conditions. Representative bright field images of monolayer cultures are shown (left panels). Whole cell lysates were probed by immunoblot for the indicated proteins and selectively phosphorylated proteins (right panels). In addition to evaluation of AKT phosphorylation, the AKT substrate site on TSC2 (T1462) and the mTor-responsive site on p70S6K (T389) were evaluated as shown. ERK1/2 is shown as a loading control. (Approximate detected molecular size: AKT-pT308, 60KDa; S6K, 70KDa; S6K-pT389; TSC2, 200KDa; TSC2-pT1462, 200KDa; ERK1/2, 42/44KDa; others as described above)

(C) U2OS and HBEC cells were transfected with the indicated siRNAs. Seventy-two hours post transfection, whole cell lysates were assessed for TBK1 expression and accumulation of phosphorylated AKT as indicated. (Detected molecular sizes were as described above).

(D) The exocyst/Ral/AKT protein-protein interaction network as derived from whole-genome yeast two-hybrid screens. Edges are colored according to the confidence score attributed to each interaction in the screens (confidence score is detailed in (Formstecher et al., 2005)): red = A, blue = B, green = C, grey =D scores.

(E) HEK293T cells were transfected with the indicated constructs. 48 hours post transfection, AKT was immunoprecipitated using anti-HA beads and coprecipitating proteins were detected as indicated. Mammalian expression constructs encoding Sec3-GFP, Exo70-GFP, Myc-Sec8 and HA-AKT were

transfected into HEK293T cells as indicated. IP indicates immunoprecipitation. WCE indicates whole cell extract. (Molecular size: Sec3, 102KDa; Exo70, 78KDa; Sec8, 110KDa; others as described above)

(F) Endogenous Sec8 was immunoprecipitated from the indicated cell lines using anti-Sec8 monoclonal antibodies. Immunoprecipitates were probed for endogenous TBK1 or IKKε as indicated. Anti-Myc monoclonal antibodies were used as a specificity control (Ctrl). (Molecular size: IKKε, a triplet centered on 80KDa; others as described above)

Figure 2. Selective contribution of TBK1 to stimulus-dependent AKT activation.

(A) Wild-type and TBK1$^{-/-}$ MEFs were incubated overnight in the absence of serum and then treated with insulin (1 μg/ml) as indicated. Whole cell extracts were probed for the indicated proteins and selectively phosphorylated proteins. Actin is shown as a loading control. (Molecular size: Actin, 45KDa; others as described)

(B) Wild-type and TBK1$^{-/-}$ MEFs were incubated overnight in the absence of serum and then treated with EGF (100 ng/ml) as indicated. Whole cell extracts were probed as in (A). (Molecular size: S6, 32KDa; S6-pS235/6, 32KDa; others as described)

(C) TBK1$^{-/-}$ MEFs were infected with lentivirus encoding GFP or TBK1. Cell were starved without serum overnight (ST O/N) and then treated with EGF (100 ng/ml) as indicated. Whole cell extracts were probed as in (A). The AKT substrate site

on GSK3β (S9) was evaluated as an indication of AKT pathway activation. (Molecular size: GSK-3β, 46KDa; GSK-3β-pS9, 46KDa; others as described)

(D) Wild-type and TBK1$^{-/-}$ MEFs were incubated cells in DMEM with 10% serum but without glucose for 2 hours followed by addition of 25 mM glucose as indicated. Whole cell extracts were probed as in (A). ND indicates the normal DMEM control. (Molecular size: as described)

(E) TBK1$^{-/-}$ MEFs were infected with lentivirus encoding GFP or TBK1. Cells were incubated in DMEM with 10% serum but without glucose for 2 hours (GD 2hr) followed by addition of 25mM glucose as indicated. Whole cell extracts were probed as in (A). (Molecular size: as described)

(F) Wild-type and TBK1$^{-/-}$ MEFs were either exposed to Sendai virus (SeV, 100 HA/ml) or treated with LPS (1 μg/ml) as indicated. Whole cell extracts were probed as in (A). (Molecular size: as described)

(G) WT and TBK1$^{-/-}$ MEFs were either maintained in the presence of serum, serum starved, or glucose deprived overnight, and then treated with Sendai virus (SeV, 100 HA/ml), EGF (100 ng/ml), or glucose (25 mM) as indicated. After 19 hours, media was collected for measuring interferonβ accumulation.

(H) WT and TBK1$^{-/-}$ MEFs were either maintained in the presence of serum (cycling cells) or serum starved 44 hr, and then treated with either EGF (100ng/ml) or FBS (10%) as indicated in the presence of BrdU (10 μM). BrdU incorporation is shown as a percentage of total nuclei.

(I) WT and TBK1$^{-/-}$ MEFs were either maintained in the presence of serum (cycling cells), serum starved, or glucose deprived. After 24hr cells were fixed and stained with DAPI. Pyknotic nuclei are shown as a percentage of total nuclei.

Figure 3. TBK1/AKT complex formation is stimulus-specific.

(A) HEK293T cells were transfected as indicated. Reciprocal co-expression/co-immunoprecipitations are shown. (Molecular size: as previously described)

(B) GST-AKT expression constructs encoding a panel of truncation variants were coexpressed with Myc-FLAG-TBK1 in HEK293T cells. Glutathione-mediated affinity isolation of the AKT variants (GST Pull-down) was used to define a minimally sufficient TBK1 interaction domain as indicated. Whole cell extracts (WCE) are shown as controls for TBK1 expression.

(C) HA-tagged TBK1 amino-terminal fragment (1-242) that encompasses the catalytic domain [TBK1 (N-terminal)] was coexpressed with either GST-AKT expression constructs [AKT(2)] or [AKT(5)]. Affinity isolation of AKT was probed for co-isolation of N-terminal TBK1as in (B).

(D) Panc-1, MDA-MB-231, Mia-Paca2, and MCF7 cells were deprived of glucose for 2 hr followed by incubation with 25 mM glucose or sorbitol as indicated. Endogenous AKT was immunoprecipitated from extracts taken at the indicated time points. Immunoprecipitates were assayed for coprecipitation of the indicated proteins. Normal mouse IgG was used as a control for specificity (IgG lanes). (Molecular size: as described)

(E) H1993 cells were either exposed to Sendai virus (SeV, 100 HA/ml) or treated with LPS (1 μg/ml), and harvested at the indicated time intervals. Co-immunoprecipitation and immunoblot were performed as in (D). Normal mouse IgG was used as a control for specificity (IgG lane). (Molecular size: as described)

Figure 4. TBK1 directly activates AKT.

(A) Myc-FLAG-tagged TBK1 was immunoprecipitated from HEK293T cells coexpressing HA-tagged AKT. Immunoprecipitates were probed for the presence of AKT and AKT-pS473 (IP). In addition, immunoprecipitates were assayed for AKT kinase activity, *in vitro*, using recombinant GST-GSK3α/β fusion peptides as substrate, and the phospho-GSK-3α/β (Ser21/9) antibody to detect substrate phosphorylation (Kinase Assay). Whole cell extracts (WCE) are shown as expression controls. (Molecular size: phospho-GST-GSK3α/β, 27KDa; others as described)

(B) HEK293T cells transfected as indicated were treated with DMSO or 20 μM LY294002 (PI3K inhibitor) for 24 hr prior to collection of protein extracts. Left panel: Whole cell extracts probed with the indicated proteins are shown. AKT-pS473 and AKT-pT308 signal intensity was quantitated as a percent of total AKT. Values shown are the mean and standard errors from three experiments. Right panel: HA-tagged AKT was immunoprecipitated and AKT kinase activity in the

immunoprecipitates was assayed as in (A).Error bars represent standard error from the mean (Right panel). (Molecular size: as described)

(C) PDPK1$^{-/-}$ HCT116 cells were transfected with plasmids encoding HA-AKT1, wild-type (WT) or kinase-dead (KD) TBK1 as indicated. Two days post-transfection, whole cell lysates were assessed for TBK1 and AKT expression, and accumulation of phosphorylated AKT as indicated. (Molecular size: as described)

(D) WT and PDPK1$^{-/-}$ DLD1 cells were transfected and treated as indicated in (C) (Left panel). Accumulation of AKT-pT308 signal intensity was normalized to total AKT signal intensity. Values are presented normalized to vector control (Right Panel). (Molecular size: as described)

(E) Sin1$^{-/-}$ MEFs were transfected with plasmids encoding wild-type (WT) or kinase-dead (KD) TBK1. Two day post-transfection, whole cell lysates were assessed for TBK1 expression and accumulation of phosphorylated AKT as indicated. (Molecular size: as described)

(F) Rictor$^{-/-}$ MEFs were transfected and treated as indicated in (C). (Molecular size: as described)

(G) Recombinant AKT and TBK1 proteins were incubated in kinase buffer with ATP at 30^{o}C as indicated. After 30min incubation, GSK3α/β fusion peptides and additional ATP were added into each reaction at 30^{o}C for an additional 30min. Reactions were separated by SDS-PAGE and immunoblotted to detect the indicated proteins and phosphorylation events. The products of kinase reactions were quantitated from multiple independent experiments. Error bars represent

standard error mean. Significance was evaluated by One-way ANOVA, Bonferroni's Multiple Comparison Test. ***, indicates $p<0.0001$.

(H) The indicated purified recombinant proteins were incubated in kinase buffer with ATP at 30^{o}C for 30min. Reactivity of recombinant AKT (top panel) with anti-phospho-AKT substrate site (R-X-R-X-X-pS/pT) antibodies (PAS) is shown (bottom panel).

(I) WT MEFs were serum starved overnight and then treated with EGF (100 ng/ml) as indicated. Endogenous TBK1 was immunoprecipitated and assayed for TBK1 kinase activity, *in vitro*, using recombinant His-AKT protein as substrate, and the anti-pS473-AKT antibody to detect substrate phosphorylation (Kinase Assay).

(J) Immunopurified Myc-FLAG-tagged TBK1 wild-type (WT) or kinase-dead (KD) was incubated with purified inactive HA-tagged AKT wild-type (WT) or kinase-dead (KD) as indicated. Kinase reactions were separated by SDS-PAGE and immunoblotted to detect the indicated proteins and phosphorylation events. (Molecular size: AKT-PAS: 70KDa; others as described)

(K) WT and PDPK1$^{-/-}$ DLD1 were infected with lentivirus encoding GFP or K-RasG12V. Three days post-infection, whole cell lysates were prepared and probed by immunoblot for the indicated proteins and selectively phosphorylated proteins. (Molecular size: as described)

Figure 5. TBK1 is required to support cancer cell tumorigenicity *in vivo*.

(A) Mia-Paca2 cells were infected with lentivirus encoding shRNAs targeting GFP (shGFP) or TBK1 (shTBK1-3, shTBK1-4 and shTBK1-6). UI indicates uninfected control. Three days post-infection, whole cell extracts were assayed for the indicated proteins. (Molecular size: as previously described)

(B) Mia-Paca2 cells were treated as in (A), and assayed for relative viability 6 days post-infection using an ATP-coupled luminescence assay (CellTiter-Glo, Promega). Bars indicated standard deviation from the mean of three independent experiments.

(C) Mia-Paca2 cells were transfected with plasmids encoding a constitutively active variant of AKT (myr-AKT) or empty vector (EV) as a control (Bellacosa et al., 1998). One-day post-transfection, cells were infected as indicated in (A) with lentivirus encoding shTBK1-4 and shTBK1-6. Five-day post-infection, cell viability was assayed as in (B). Significance was evaluated using the student's two-tailed T-test.

(D) $1x10^6$ Mia-Paca2 cells uninfected (n=5) or stably expressing GFP (n=4) or shRNA constructs targeting TBK1 (TBK1-3, n=4; TBK1-6; n=4) were injected into the pancreas of SCID mice. All cells were collected two days post lentiviral infection and viability was confirmed by trypan blue exclusion. At this time-point, TBK1 depletion has not proceeded to the point that begins to engage cell death. Animal health and tumor growth was monitored and a cohort of animals sacrificed on Day 49 post tumor cell injection. Total tumor incidence is shown.

(E) Pancreas weight (tumor burden) was normalized to total body weight at the end of the study and is displayed as % of body weight.

(F) MDA-MB-231 cells uninfected or stably expressing GFP or shRNA targeting TBK1 (TBK1-6) (n=5/group) were injected into the mammary fat pad of female SCID mice. Again, all cells were collected two days post lentiviral infection and viability was confirmed by trypan blue exclusion. Animal health and tumor volume were followed throughout the duration of the experiment.

(G) Tumor burden at the time of sacrifice is displayed as final tumor weight.

(H) Metastatic incidence.

(D-H) *, indicates $p<0.05$; and ***, indicates $p<0.005$ vs. uninfected control by ANOVA with a Bonferroni correction for multiple comparison testing.

Figure 6. Pharmacological inhibition of TBK1 impairs AKT signaling.

(A) Structure of Compound II.

(B) IC_{50} values for *in vitro* inhibition of the indicated purified recombinant kinases by Compound II.

(C) Primary macrophages from mouse bone marrow were treated with LPS and increasing concentrations concentration of Compound II. LPS induced accumulation of interferonβ (IFNβ) and interferonβ target gene (IP10 and Mx1) mRNAs were measured by quantitative PCR and shown as percent of inhibition. Error bars represent S.D.M. from triplicate experiments.

(D) HeLa cells incubated in the indicated concentrations of Compound II were stimulated with 10 ng/ml TNFα for 10 minutes (p65 assays), or transfected with poly I:C for 2 hours (IRF3 assays), followed by immunofluorescence-based detection of IRF3 and p65 nuclear accumulation. Nuclear accumulation is plotted as percent of control (POC). Error bars represent S.D.M. from triplicate analysis.

(E) Wild-type MEFs were incubated cells in DMEM with 10% serum but without glucose for 2 hours. Cells were then pretreated with 2 μM Compound II for 30 minutes as indicated followed by addition of 25 mM glucose as indicated. Whole cell extracts were prepared post glucose stimulation and immunoblotted as shown. (Molecular size: as described)

(F) Asynchronous proliferating cultures of HCC44 cells were exposed to the indicated concentrations of Compound II for 30 minutes. Whole cell extracts were immunoblotted for detection of the indicated proteins and phospho-proteins. (Molecular size: as described)

(G) $Sin1^{-/-}$ and $Rictor^{-/-}$ MEFs were pretreated with DMSO or Compound II for 30 minutes as indicated, followed by exposure to LPS (1 μg/ml) or Sendai virus (SeV, 100 HA/ml). Whole cell extracts prepared at the indicated time-points were immunoblotted for detection of AKT activation. (Molecular size: as described)

(H) Whole cell extracts from HCC44, A549 and Mia-Paca2 cells exposed to the indicated concentrations of Compound II or LY294002 for 24 hours were

immunoblotted to detect consequences on AKT pathway activation. (Molecular size: cleaved-PARP: 89KDa; others as described)

Figure 7. TBK1 sensitivity in non small cell lung cancer.

(A) The indicated cell lines were infected with lentivirus encoding shRNAs targeting GFP or two independent shRNAs targeting TBK1 as indicated. Relative cell viability was assayed 6 days post infection as in Figure 5. Whole cell extracts from parallel infections were collected and probed for the indicated proteins. (Molecular size: E-Cadherin, 135KDa; others as previously described)

(B) Following a 96-hour exposure to the indicated concentrations of Compound II, A549 and H441 cell viability was measured as indicated. Bars represent standard error from the mean of three independent experiments.

(C) The indicated cell lines were exposed to DMSO or 2 μM Compound II for 24 hours. Cells were then labeled with FITC-conjugated Annexin V, and scored by FACS. Values shown in the heat-map represent fold-induction of Annexin V positive cells over the DMSO controls (Δ).

(D) Whole cell extracts from cells treated for 24 hours as in (C) were immunoblotted as indicated. Lysates were loaded based on equivalent cell numbers for each sample. (Molecular size: as previously described)

Figure 1. Ou et al. 2010

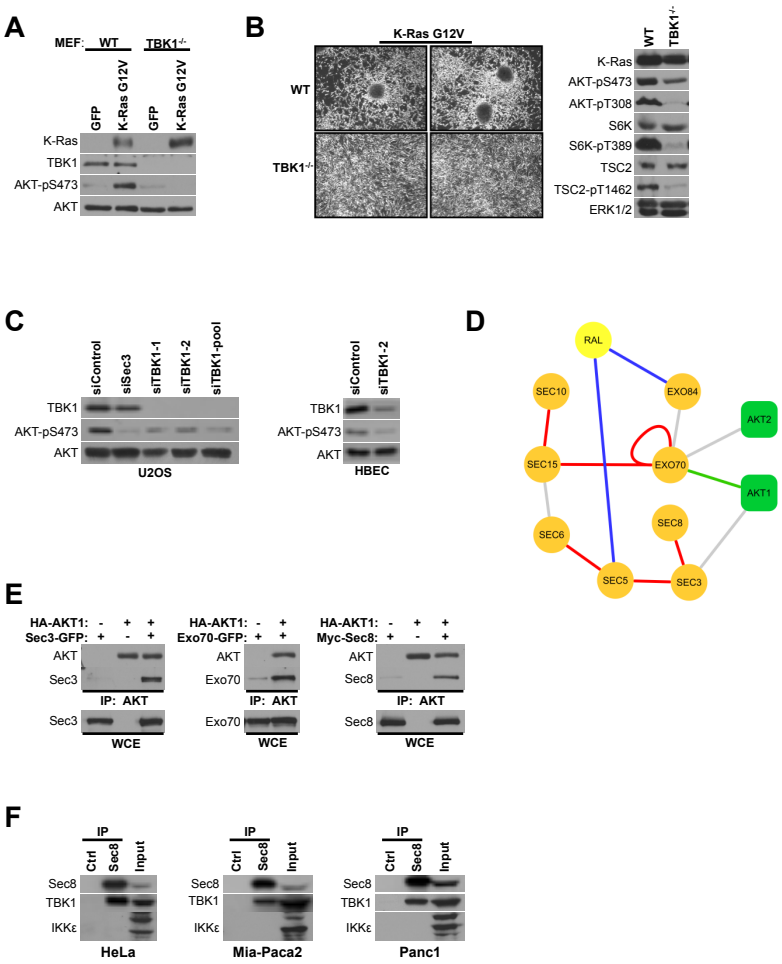

Figure 2. Ou et al. 2010

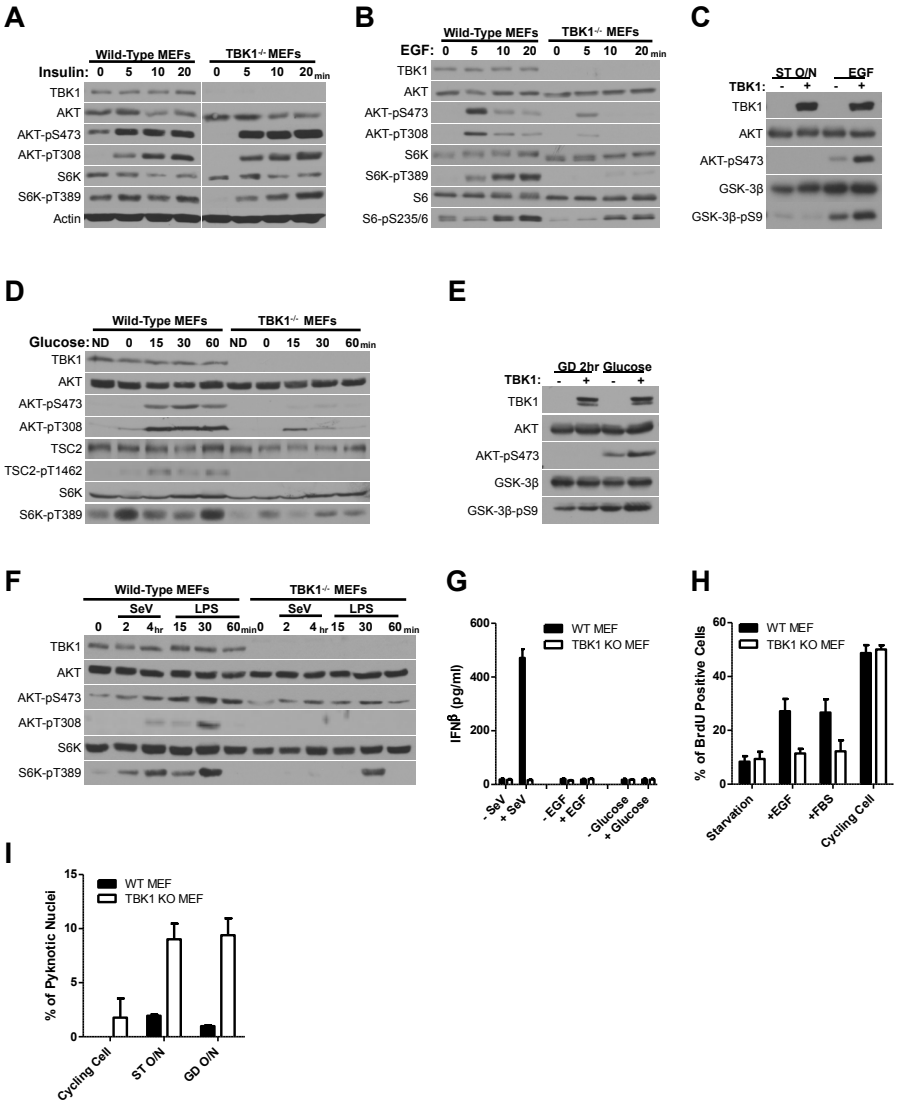

Figure 3. Ou et al. 2010

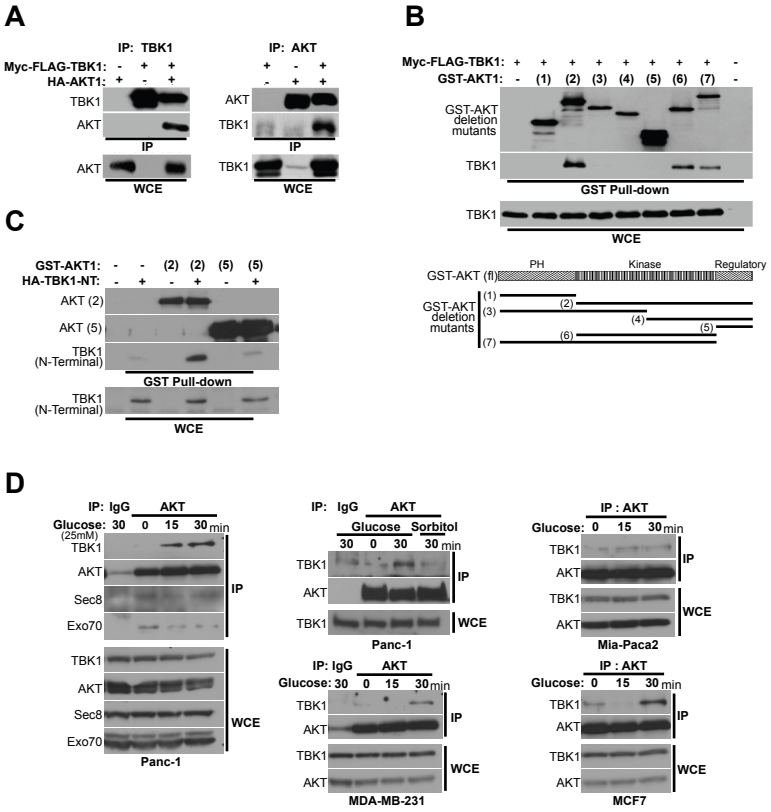

Figure 4. Ou et al. 2010

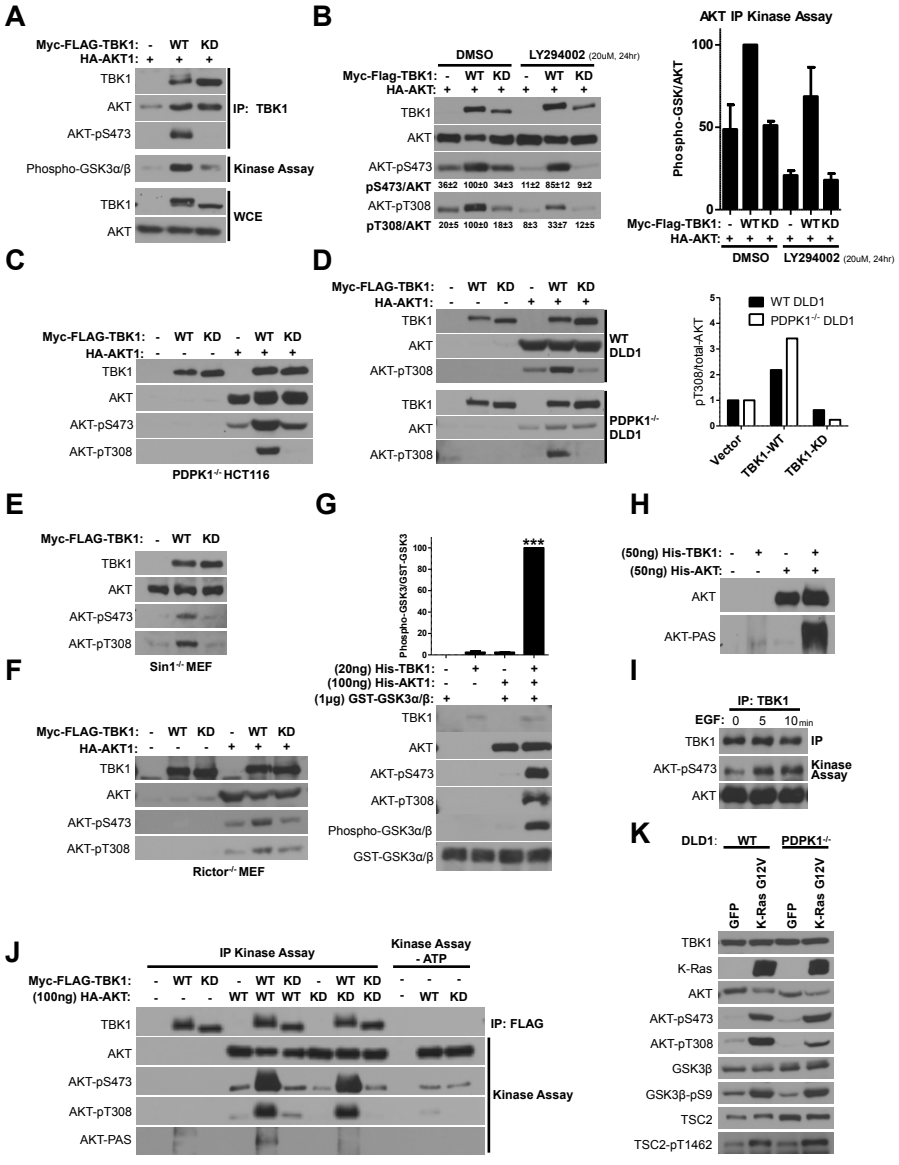

Figure 5. Ou et al. 2010

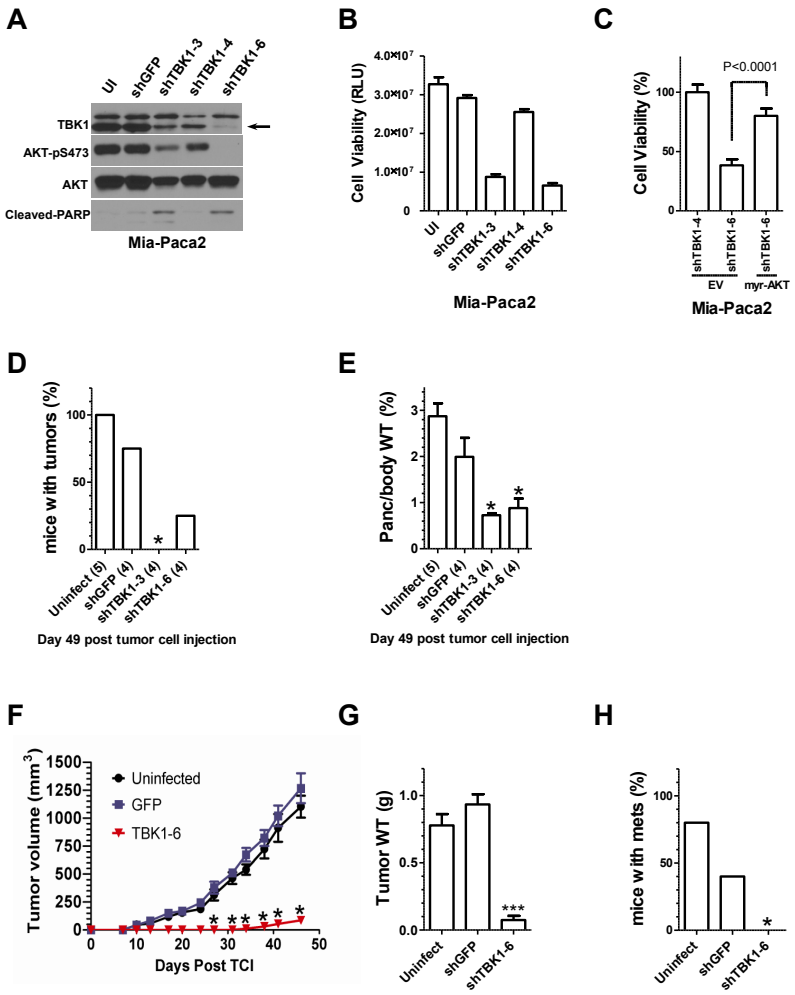

Figure 6. Ou et al. 2010

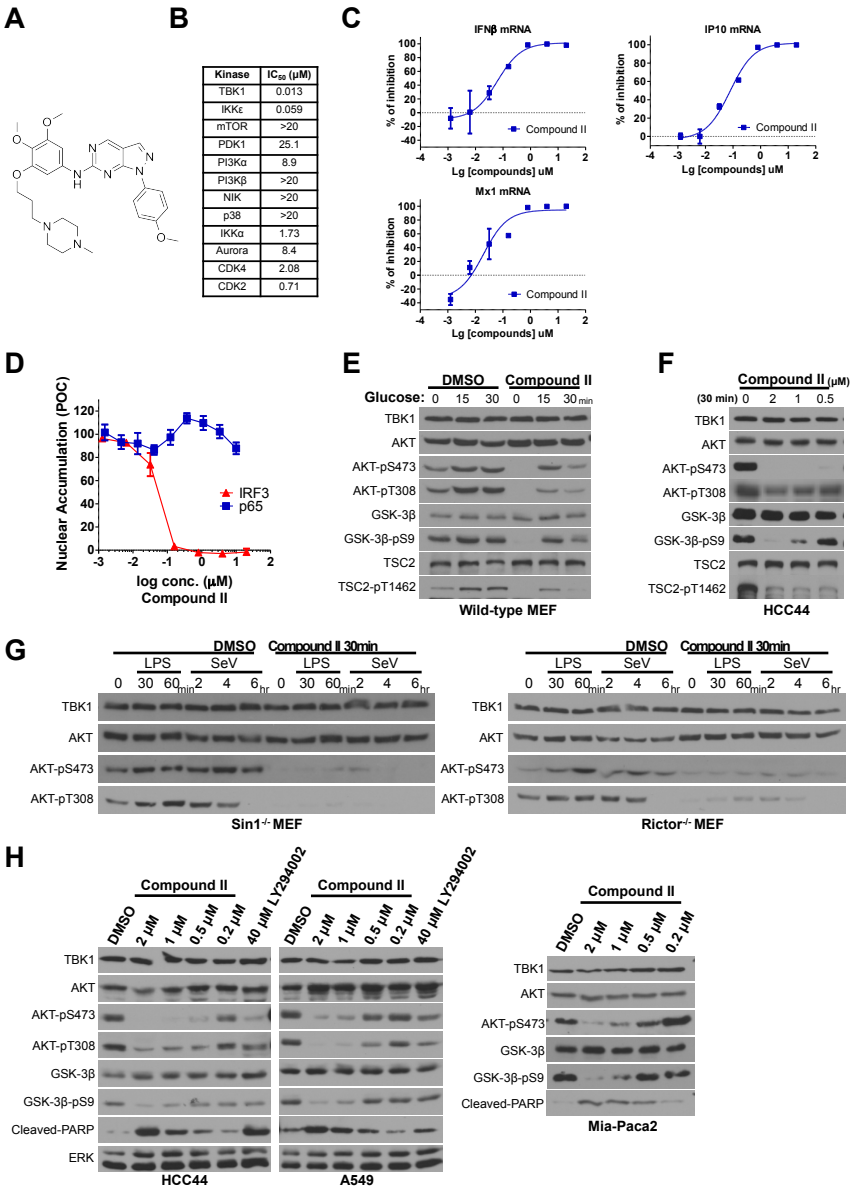

Figure 7. Ou et al. 2010

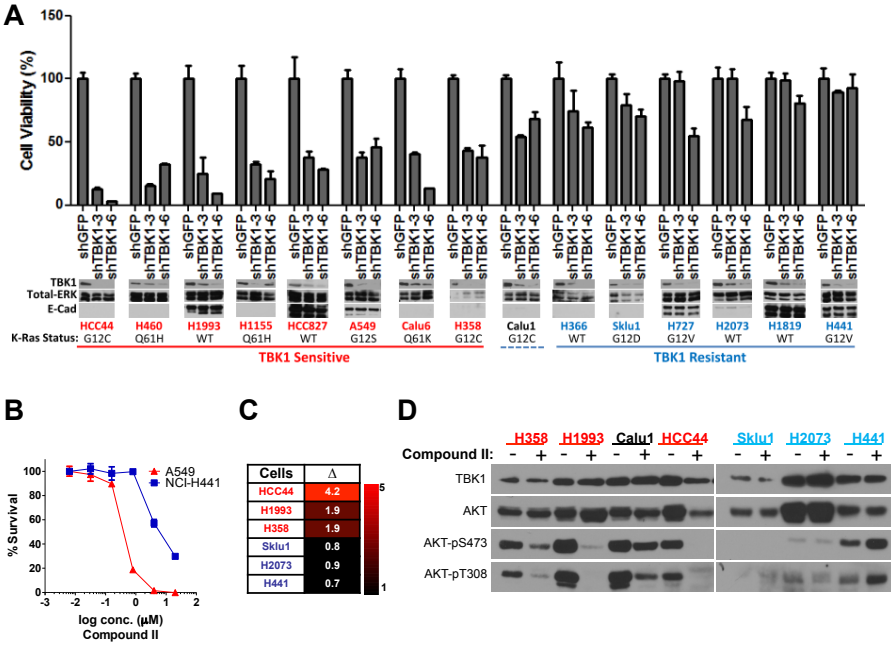

Experiments and Figures Contributed by me:

Figure 5

Figure 6

Figure 7

CHAPTER THREE

The Sec6/8 (a.k.a. Exocyst) Complex Regulates DNA Repair Fidelity

Michael J. Torres[1], Raj K. Pandita[2], Ozlem Kulak[1], Rakesh Kumar[2], Etienne Formstecher[3], Yingming Zhao[4], Lawrence Lum[1], Tej K. Pandita[2*], and Michael White[1*]

[1]Department of Cell Biology, University of Texas Southwestern Medical Center, Dallas, Texas

[2]Department of Radiation Oncology, University of Texas Southwestern Medical Center, Dallas, Texas

[3]Hybrigenics, Inc., 75 014 Paris, France

[4]Ben May Department for Cancer Research, The University of Chicago, Chicago, Illinois 60637, USA.

Key words: Genomic Instability, DNA Repair, Exocyst, Sec8, Exoc4, ATF2, RNF20, Histone Acetyl Transferase, p53, Chromatin

Short title: Exocyst-dependent Regulation of the DNA Damage Response.

*Correspondence: Michael.White@UTSouthwestern.edu,

Tej.Pandita@UTSouthwestern.edu

Abstract

The exocyst is a heterooctomeric protein complex well appreciated for its role in dynamic assembly of specialized plasma membrane and endomembrane domains. Accumulating evidence indicates this macromolecular machine also serves as a physical platform that coordinates organellar assembly with activation of parallel regulatory cascades required to support biological systems such as host defense signaling, cell fate, and energy homeostasis. The isolation of multiple components of the DNA damage response (DDR) within the human exocyst protein-protein interaction network, together with the identification of Sec8 as a suppressor of the p53 response, prompted an investigation of functional interactions between the exocyst and the DDR. We found that exocyst perturbation resulted in a radioresistance phenotype to ionizing radiation (IR) that was associated with accelerated resolution of DNA damage. This occurred at the expense of genomic integrity, as enhanced recombination frequencies correlated with the accumulation of aberrant chromatid exchanges. Exocyst-dependent modulation of the DDR is, at least in part, through restraint of the associated chromatin modifiers ATF2 and RNF20. Exocyst perturbation resulted in aberrant accumulation of ATF2 and RNF20; the promiscuous accumulation of DDR-associated chromatin marks; and IR-induced increased Rad51 repairosomes. Thus, the exocyst indirectly supports DNA repair fidelity by limiting formation of repair chromatin in the absence of a DNA damage signal.

Introduction:

Sec8 (or EXOC4) is a member of the heterooctomeric exocyst complex comprised of

seven other subunits named Sec6, Sec5, Exo70, Exo84, Sec3, and Sec10. First characterized in yeast[1], the mammalian exocyst complex has been directly implicated in the trafficking of post Golgi-derived vesicles to the basolateral membrane of polarized epithelial cells[21] as well as participating in the innate immunity response through action of TBK1[22]. Additional observations implicate the exocyst complex in cytokinesis by directing vesicles to specific membrane domains[14]. The exocyst complex has also been shown to be essential in the autophagy pathway by directing the assembly of autophagy components in response to nutrient availability[13]. In nutrient rich conditions, mTORC1 (mammalian target of rapamycin complex 1) interacts with a Sec5-exocyst complex that promotes inactivation of ULK1, which inhibits ULK1 mediated autophagy. Conversely, in nutrient deficient conditions and in a RalB-dependent manner, an exocyst subcomplex of ULK1(unc-51-like kinase 1) and Exo84 facilitate assembly of the autophagy machinery[13]. Collectively, this evidence supports the exocyst as a spatial- and temporal-signaling platform that responds to diverse cellular cues.

There is also strong evidence linking the exocyst to oncogenesis and cancer cell survival[5,23]. In a study seeking to find mutations that drive oncogenic events in colorectal cancer, mutations in Sec8 were identified, suggesting that Sec8 mutations are associated with mechanisms driving oncogenesis[20]. Corroborating the importance of Sec8 in cancer was a study that observed high deletion of Sec8 in colorectal tumors of African Americans patients[7]. Previous work from our lab established that a TBK1-exocyst interaction in cancer cells drives AKT activation, resulting in aberrant proliferation[22,74].

However, overexpression of Sec8 has also been implicated in promoting a tumorigenic environment by upregulating the expression of matrix metalloproteases, which are associated with tumor invasion[5]. Thus, proper maintenance of exocyst function may be crucial to suppressing tumorigenic activity.

To examine additional mechanisms of the exocyst's contribution to oncogenesis we examined the molecular composition of exocyst protein-protein interactions using an immunoprecipitation/mass spectrometry and yeast two-hybrid approach described previously[22,69]. Through this approach we identified several canonical DNA damage response proteins including 53bp1 that interact with the exocyst complex. 53bp1 has been identified as an important driver of repair choice either through non-homologous end-joining (NHEJ) or homologous recombination (HR) [75-77]. We found that depletion of Sec8 results in an altered response to DNA damage agents such as irradiation (IR), characterized by increased resolution of gH2AX and increased resistance to IR. We find that this alteration results in increased recombination and increased genomic instability. Given that histone modification and chromatin microenvironments are emerging as important drivers of repair choice[78,79], we examined several key DNA damage responsive histone-modifying proteins, including ATF2 and RNF20, alterations of which are associated with driving oncogenesis[80-83]. We found dysregulation of these two proteins upon Sec8 depletion, in the absence of exogenous DNA damage, suggesting that loss of Sec8 alters the chromatin microenvironment and may account for the increased error-prone DNA repair observed.

Results

Physical and functional association of Sec8 with DNA damage response proteins.

TP53 loss of function mutations occur in 50% of colorectal cancers, suggesting suppression of a p53 response is a common feature leading to initiation and/or progression of that disease[84]. In tumors that retain wild-type p53, somatic alterations have been identified within the p53 regulatory network that are functionally equivalent to p53 loss of function; either through enhanced destabilization of p53 due to post-translational modifications or through inactivation of p53 effectors[85,86]. To potentially identify previously unrecognized proteins that are functionally linked to the p53 tumor suppressor network, we screened the consequence of siRNA-mediated depletion of 140 candidate colorectal cancer genes (CAN-genes[87]) on p53 promoter activity in two independent p53 positive colorectal cancer cell lines (HCT116, RKO)(Figure 1A). Among the top 10 enhancers of the pp53-TA-Luc reporter, in both cell lines, were siRNAs targeting the exocyst subunit Exoc4/Sec8L1 (hereafter referred to as Sec8). Depletion of Sec8 also induced expression of the endogenous p53 target genes Cdkn1a and Bbc3 (Figure 1B) suggesting that Sec8 depletion either induces or de-represses a canonical p53 response. Notably, 33 proteins implicated as participants in p53-associated DNA damage responses were identified within an exocyst protein-protein interaction network (Figure 1C). This exocyst PPI was constructed with a combination of yeast two-hybrid screens and mass spectrometry of immuno-isolated endogenous Sec8[22,69], and contains elements of the FancD2-FancI complex which participate in Inter-Strand Crosslink (ICL) repair[88];

members of the CAK complex involved in Transcription-Coupled Nucleotide Excision Repair (TC-NER)[89]; members of the Non-Homologous End-Joining (NHEJ) pathway; members of the Bre complex (RNF20/RNF40) involved in DNA repair-associated chromatin remodeling[82]; and 53BP1, a key adaptor protein involved in regulating DNA DSB repair pathway choice[75,90,91].

The Sec8/53BP1 interaction was recapitulated by endogenous co-immunoprecipitation (Co-IP) from HBEC 3KT cells using anti-Sec8 antibodies (Figure 1D), and by co-expression/co-immunoprecipitation (Co-IP) of epitope tagged proteins expressed in HEK 293 cells (Figure 1E). The endogenous complex was sensitive to IR, suggesting the Sec8/53BP1 interaction may be disrupted upon detection of DNA damage (Figure 1D). While predominantly a cytosolic complex, nuclear roles for components of the exocyst have been described[92]. Consistent with this, we found a subpopulation of endogenous Sec8 localized with 53BP1-positive nuclear punctae in proliferating cell cultures (Figure 1F).

53BP1 Depletion Induces Autophagy That is Beclin1 dependent but Exocyst Independent

The interaction of exocyst and DDR proteins led us to consider functional crosstalk between these regulatory systems. Given the recently described mechanistic interactions of both exocyst and DDR proteins with the core machinery required for autophagosome formation and maturation[13,93-95], we first examined the contribution of 53BP1 to exocyst-

dependent autophagic flux. A U2OS cell line with stable expression of GFP-LC3 was used for these studies. Lipidated LC3 coats the membranes of nascent autophagosomes and is proteolytically degraded in mature autophagolysosomes; thus serving as an indicator of autophagy dynamics[96]. Depletion of 53BP1, in these cells, reduced accumulation of total GFP-LC3 (Figure 2A) in nutrient-replete culture conditions and enhanced accumulation of GFP-LC3 punctae in the presence of chloroquine (Figure 2B). In addition, GFP-LC3 accumulation in 53BP1-depleted cells was rescued by codepletion of the core autophagy protein Beclin1; suggesting the observed alterations in GFP-LC3 accumulation are autophagosome-dependent (Figure 2C). Together, these observations indicate induction of autophagic flux upon depletion of 53BP1. We have previously demonstrated that the exocyst complex supports starvation-induced autophagosome biogenesis through Exo84 subunit interactions with ULK1 and Beclin1[13]. As expected, cells depleted of Exo84 showed significant accumulation of GFP-LC3 as would result from inhibition of autophagic flux (Figure 2D). However, the enhanced autophagic flux observed upon 53BP1 depletion was independent of Exo84 expression (Figure 2D). Likewise, the Sec8/53BP1 interaction was insensitive to alteration of nutrients, suggesting an independent contribution of 53BP1 to the regulation of autophagy (Figure 2E). p53 itself has been identified as an inhibitor of autophagosome biogenesis, through an undetermined mechanism, independent of its role as a transcription factor[97]. The consequence of 53BP1 depletion on total LC3-GFP accumulation was similar in magnitude as that observed upon depletion of p53 and codepletion of both had no further detectable consequences (Figure 2F); consistent with participation of 53BP1 in p53-

inhibition of autophagic flux. Given the seemingly independent contributions of 53BP1 and the exocyst to the regulation of autophagy, we instead considered the possibility that exocyst proteins participate together with 53BP1 in the DNA-damage response.

Sec8 Supports DDR Fidelity

Phosphorylation of H2AX on serine 139 (γH2AX) is one of the earliest detectable steps in the recruitment of repair factors to sites of DNA damage, particularly DNA double-stranded breaks, and occurs in response to activation of most DNA repair pathways[98]. Therefore, we first asked if the γH2AX response was perturbed by Sec8 depletion. Upon exposure of HBEC 3KT cells to IR, we found that γH2AX was equivalently detectable by 10 minutes in both Sec8 depleted cells and controls. However, Sec8 depleted cells had markedly decreased residual γH2AX at later time points, suggesting abbreviated DNA damage processing as compared to controls (Figure 3A). This phenotype was recapitulated in U2OS cells with both 1 Gy and 5 Gy IR exposure; was reproducible with 3 out of 4 independent siRNA oligonucleotides targeting Sec8; and was recapitulated by depletion of the exocyst subunits Sec6, Sec5, Sec10, and Sec3 (Figure 3 B-D). Sec8 depletion also significantly reduced the accumulation of DDR foci in response to replication-coupled DNA damage or CPT (Figure 3E-F), indicating the phenotype is not specific to the DNA damaging agent employed. At single cell resolution, we were surprised to find that Sec8 depletion resulted in a significant increase in IR-induced γH2AX foci/nucleus by 10 minutes post exposure relative to control (Figure 3G). This was followed by a significant decrease in γH2AX foci/nucleus in Sec8 depleted cells

relative to control by 1hour post irradiation (Figure 3G). The altered γH2AX kinetics were independent of any gross differences in cell cycle kinetics, as Sec8 depletion did not alter G1-S-G2/M distributions in proliferating cultures (Figure 3H) or DNA-damage induced cell cycle arrest (Figure 3I). Together these observations suggest that Sec8 depletion sensitizes cells to DNA break formation or detection in a manner that also alters the persistence of the DNA damage response or resolution of the breaks themselves.

We next directly examined the extent and persistence of IR-induced DNA damage upon exocyst perturbation. Analysis of DNA fragmentation in neutral comet assays revealed that Sec8 depleted cells displayed a significant decrease in tail length as compared to control cells 30 minutes post-exposure to 10 Gy (Figure 4A). Furthermore, IR induced cell killing as determined by clonogenic survival post IR-exposure was reduced in Sec8-depleted cells (Figure 4B). Together, these observations indicate that Sec8-depletion enhances DSB resolution or increases resistance to DSB formation. Notably, analysis of metaphase spreads from irradiated cells revealed a reduced frequency of persistent DNA breaks in Sec8 depleted cells (Figure 4C Blue Arrows). However, the frequency of chromatid exchanges (triradials and quadriradials) was significantly increased in these same cells (Figure 4C Red Arrows). This phenotype is reminiscent of chromosomal aberrations that occur as a consequence of altered NHEJ (non homologous end joining) and an associated increased frequency of HR (homologous recombination)[76,99]. We therefore evaluated HR frequencies using a GFP reporter system to monitor resolution of a site-specific break induced by the rare-cutting endonuclease I-SceI[100]. Within this

system, depletion of Sec8 significantly increased in the percentage of cells expressing GFP relative to control (Figure 4D), consistent with increased HR. Finally, we assayed fluorescent nucleotide analog incorporation into individual DNA fibers to follow replication fork stalling and origin of replication firing in response to replicative DNA damage[101]. To measure stalled replication kinetics, cells were pulse labeled with 5-iododeoxyuridine (IdU), exposed to hydroxyurea for 1, 4, or 24hr to deplete the nucleotide pool and then allowed to recover in the presence of 5-chlorodeoxyuridine (CIdU). To measure new replication origins, cells were pulse labeled with IdU, eposed to hydroxyurea, and then pulse-labeled with CldU for 1, 4, and 24hr as previously described[102,103]. Within this system, stalled replication forks are indicated by IdU positive/CldU negative fibers, and new origins of replication are indicated by IdU negative/CldU positive fibers. Equivalent accumulation of stalled replication forks (Idu only tracks) were observed in both control and Sec8 siRNA cells (Figure 4E), suggesting that Sec8 depletion does not deflect damage-induced replicative arrest. However, Sec8 depleted cells displayed an increased frequency of new replication origins (CldU only tracks) by 4hr and 24hr post exposure to HU (Figure 4E). The later observation is consistent with faster resolution of DSB-induced cell cycle arrest in Sec8 depleted cells. These cumulative observations indicate that Sec8 depletion alters both the kinetics and fidelity of DNA repair.

Sec8 Regulates Histone Modifying Proteins ATF2 and RNF20

In an effort to parse key effectors, driving the altered DDR kinetics and genomic

instability seen upon Sec8 loss, we queried available synthetic genetic array (SGA) data from yeast for genetic interactions with exocyst mutants. Analysis of the SGA resource using pairwise correlation coefficients allows for clustering of significant (r = >0.1) biological relationships[104]. Among the exocyst mutants that were not single gene lethal[105,106], we identified a functional cluster centered on Sec3 that contained additional subunits of the exocyst and the histone acetyltransferase HPA2, which suggests the exocyst complex participates in regulation of histone modification (Figure 5A; Sec15 r = 0.282, Sec10 r = 0.278, Exo70 r = 0.23, HPA2 r =0.221). Notably, yeast HPA2 and the human exocyst-interacting protein ATF2 have overlapping biochemical specificity for histone H4 lysine acetylation. Together with Tip60 (KAT5), ATF2 histone acetyl transferase activity supports homologous recombination-mediated DNA damage repair[107,108]. We found that Sec8 depletion resulted in a marked accumulation of ATF2 protein in the absence of altered mRNA transcript concentrations (Figure 5B-C). We next examined the exocyst PPI for E3 ligases that are predicted to interact with the exocyst. We reasoned that regulation of E3 ligases by the exocyst might account for accumulation of proteins seen upon depletion of Sec8. Huwe1 and Ubr5 were identified as potential exocyst interactors, both of which participate in regulation of the DNA damage response[109,110]. Downregulation of Huwe1 has been shown to promote IR resistance through regulation of BRCA1[111]. Upon depletion of Huwe1 we see marked elevation of ATF2 protein concentration, which suggests that ATF2 may be a substrate of Huwe1 (Figure 5D). The elevated ATF2 protein concentration corresponded to enhanced nuclear accumulation of ATF2 and enhanced IR-induced phosphorylation of ATF2 on its ATM

kinase substrate sites (S490/S498); suggesting increased ATF2 activity (Figure 5E)[112,80]. This was mirrored by accumulation of Tip60, which interacts with ATF2 to support HAT activity and DNA repair pathway specification (Figure 5F). Importantly, RNF20 protein also accumulated upon Sec8 depletion independently of altered transcript levels (Figure 5G). As previously reported, aberrant accumulation of this E3 ligase is associated with genomic instability[83]. We found that RNF20 accumulation correlated with ubiquitination of its target protein H2B on K120, together with accumulation of H2BK120ub-dependent tri-methylation of H3K4 (Figure 5H). These histone modifications are required for proper chromatin remodeling and subsequent recruitment of DNA repair factors in both the NHEJ and HR pathways[82,113]. The significant increase in HR-associated Rad51 foci upon Sec8 depletion indicated that these altered histone modifications are affecting repair pathway specification (Figure 5I). Together, these results suggest that Sec8 normally restrains chromatin remodeling factor activity in support of DNA repair fidelity.

Discussion:

Collectively, the observations described here suggest the exocyst complex helps support DNA repair fidelity, at least in part, by restraining the activity of chromatin remodeling factors in the absence of appropriate DNA damage signaling (Figure 6). Upon depletion of Sec8, the promiscuous accumulation of repair chromatin appears to serve as a priming event for the generation and resolution of DNA damage repair foci. While conferring a modicum of resistance to IR, the resulting enhanced DNA repair activity is low fidelity and generates aberrant chromatin rearrangements. Thus exocyst perturbation results in a

mutator phenotype. Of note, somatic mutations in Sec8 have been identified in colorectal cancers, and Sec8 deletions are significantly overrepresented in colorectal tumors of African Americans patients[7]. If associated with defective DDR activity, these alterations could both confer resistance to radiotherapy and enhance genomic instability within the tumor harboring them. A potentially related clinical correlation is the association of germline Sec8 variants with radiation proctitis in a GWAS study of prostate cancer patients (M Parliament, (University of Alberta, Edmonton, AB, Canada) personal communication with permission). A key focus for future investigation is the nature of the selective pressure leading to the physical and functional association of the exocyst and canonical DNA repair machinery. By extrapolation from the recently described mechanistic participation of the exocyst in host defense signaling and autophagy, we suspect this macromolecular machine serves as a spatially constrained platform from which to effectively coordinate localized enzyme/substrate interactions[13,22,74]

Acknowledgements

We thank A. Diehl and the UT Southwestern Live Cell Imaging Facility for their assistance. We also thank J. Minna and X. Wang for providing reagents used in this study. This work was supported by grants from the Welch Foundation (I-1414 to M.W), grants from the National Institutes of Health (CA71443 and CA129451 to M.W).

Figure 1: The exocyst interacts with DNA damage response proteins. (A) The consequence of siRNAs targeting candidate colorectal cancer genes on p53-dependent luciferase reporter activity was assessed in HCT116 and RKO cells. SiRNA pools were rank ordered by effect size. Values indicate the mean and standard deviation of the ratio of p53-dependent firefly luciferase activity to constitutively expressed *Renilla* luciferase activity (N=3). **(B)** Relative Cdkn1a, Bbc3 (left) and Sec8 (right) mRNA concentrations upon exposure to the indicate siRNAs. Error bars indicate SEM from N=3. **** indicates p= <0.0001 by student's t-test. **(C)** The exocyst/DNA damage response protein-protein interaction network as derived from whole-genome yeast two-hybrid screens and IP/Mass Spectroscopy. Edge colors indicate literature-based interactions (yellow) or 2H screen confidence scores (confidence score is as detailed previously[69]): red, A; blue, B; green, C; orange, D. Unconnected nodes indicate proteins exclusively detected by IP/MS. **(D)** Endogenous Sec8 was immunoprecipitated from HBEC 3KT cells using an anti-Sec8 monoclonal antibody. Immunoprecipitates were probed for endogenous 53bp1 as indicated. Anti-HA monoclonal antibodies were used as a specificity control. 10ug of soluble fraction was loaded as an input control (IN). **(E)** HEK293T cells were transfected with the indicated constructs. 72 hr post transfection, Flag-53bp1 was immunoprecipitated using anti-Flag antibody-bead conjugates and Myc-Sec8 was probed with anti-Myc antibody. IP: immunoprecipitation. WCL: whole-cell lysate. **(F)** Colocalization was assessed by confocal microscopy with indicated antibodies using a TCS SP5 confocal microscope with a sequential 3-channel scan. siRNA of Sec8 was used as a control for specificity of colocalization. Representative images from 2 independent

experiments are shown. Arrow-heads in the enlarged boxes (left panels) indicate spontaneous 53BP1- and Sec8-positive nuclear punctae. Image scaling is as indicated by the scale bars (22 microns).

Figure 2: 53bp1 suppresses exocyst-independent autophagy. (A) Single cell fluorescence intensity distributions are shown for U2OS GFP-LC3 cells 72hr post-transfection with the indicated siRNAs. Histogram is representative of 3 independent experiments. **(B)** Image-based quantification of GFP-LC3 punctae/cell after treatment with 50 mM Chloroquine in U2OS cells 72hr post-transfection with the indicated siRNAs. Bars indicate the mean and SEM from 3 independent experiments. MM 36.71 ± 1.945 N=106; Sec8 60.23 ± 2.761 N=103. *** indicates p= <0.001 . **(C)** (Top) Population means from flow cytometry (as in A) of GFP-LC3 in U2OS cells 72hr post-transfection with the indicated siRNAs. Bars indicate the log2 mean ± SEM fluorescence intensity normalized to control siRNA (MM). N=3. * indicates p= 0.0121, ** indicates p= 0.0060 (Lower) Immunoblot confirmation of target knockdown. Results shown are representative of 3 replicates. **(D)** (Top) Population means from flow cytometry (as in A) of GFP-LC3 in U2OS cells 72hr post-transfection with the indicated siRNAs. Bars indicate the log2 mean ± SEM fluorescence intensity normalized to control siRNA (MM). N=3. *** indicates p= 0.0002, * indicates p= 0.0356, *** indicates p= 0.0002. (Lower) Immunoblot confirmation of target knockdown. Results shown are representative of 3 replicates. **(E)** Endogenous Sec8 was immunoprecipitated from HBEC 3KT cells following a 4-hour incubation in nutrient replete medium (RPMI) or EBSS as indicated. Immunoprecipitates were probed for endogenous 53bp1 as indicated. Anti-HA

monoclonal antibodies were used as a specificity control. **(F)** Single cell fluorescence intensity distributions are shown for U2OS GFP-LC3 cells 72hr post-transfection with the indicated siRNAs. Histogram is representative of 2 independent experiments.

Figure 3: Sec8 modulates the γH2AX response to DNA damage. (A) Immunoblots from whole-cell lysates with indicated antibodies in HBEC 3KTcells after exposure to 5 Gy irradiation and incubation for indicated time points 72hr post-transfection with the indicated siRNAs. Results shown represent >3 independent experiments. **(B)** Immunoblots from whole-cell lysates with indicated antibodies in U2OS cells after exposure to 1 and 5 Gy irradiation and 30 min incubation 72hr post-transfection with the indicated siRNAs. **(C)** Immunoblots from whole-cell lysates with indicated antibodies in U2OS cells after exposure to 5 Gy irradiation and 1hr incubation 72hr post-transfection with the individual Sec8 siRNAs. **(D)** Immunoblots from whole-cell lysates with indicated antibodies in HBEC 3KT cells after exposure to 10 Gy irradiation and 1hr incubation 72hr post-transfection with the individual Exocyst subunit siRNAs. **(E)** Image-based quantification of APH-induced 53bp1 foci in HBEC 3KT cells 72hr post-transfection with indicated siRNAs. Cells with > 3 53bp1 foci, as observed by confocal microscopy were scored as positive. Bars indicate mean and SEM from 2 independent experiments. MM 86.09 ± 1.444 N=407; Sec8 27.48 ± 2.900 N=354. *** indicates p= <0.0001. **(F)** Immunoblot of whole cell lysates from HBEC 3KT cells following exposure to 100 nM CPT followed by addition of fresh medium without drug and incubation for 2hr. Results are representative of 2 independent experiments. **(G)**

Representative images of γH2AX foci in U2OS cells after irradiation 72hr post-transfection with indicated siRNAs (Top). Image-based quantification of γH2AX foci in U2OS cells, following 1 Gy irradiation and incubation for indicated time points 72hr post-transfection with indicated siRNAs. Foci/cell are indicated with box and whisker plots (min to max). (Bottom). MM 10 min 23.16 ± 0.6484 N=96; Sec8 10 min 28.43 ± 0.7831 N=77, **** indicates p= <0.0001; MM 1hr 23.48 ± 0.6752 N=81; Sec8 1hr 20.65 ± 0.5598 N=81, ** indicates p= <0.0015. **(H)** Histogram of DNA content as indicated by propidium iodide ((PI (FL3-H)) fluorescence intensity of U2OS cells 72 hr post-transfection with indicated siRNA. Results shown are representative of 2 independent experiments. **(I)** 72 hours post-transfection with indicated siRNAs, U2OS cells were fixed and stained with PI and anti-phospho-MPM-2 one hour after exposure to the indicated doses of IR. Bars indicate the percentage of diploid p-MPM-2 positive cells as detected by FACS. Error bars indicate SEM.

Figure 4: Sec8 depletion accelerates low-fidelity DNA Repair (A) Representative images of DNA damage (neutral comet tail) following irradiation of U2OS cells 72hr post-transfection with indicated siRNAs. (Left). Quantification of comet tail length/cell in pixels is shown (right). MM 28805 ± 927.0 N=91; Sec8 18866 ± 841.3 N=96, *** indicates p= <0.0001). **(B)** Ionizing radiation response in U2OS cells seeded and irradiated at indicated doses 72hr post-transfection. 10 days post IR exposure, colonies with > 50 colonies were counted and survival fractions were calculated. Results shown represent 3 independent experiments performed in triplicate. (4gy and 8gy: * indicates p=

<0.05). (Top). Western blot confirmation of knockdown (Bottom). **(C)** Representative images of metaphase spreads in colcemid-treated (3 hr) U2OS cells following exposure to 1 Gy irradiation and 30 min incubation with indicated doses 72hr post-transfection. Blue arrows indicate breaks and red arrows indicate exchanges (Top). Quantification is shown below. Results shown represent 2 independent experiments. * indicates p= <0.05. **(D)** HR frequency is shown as a percent accumulation of GFP+ MCF7 cells following transfection with the indicated siRNAs and I-Sce1 plasmid. * indicates p= <0.01. **(E)** Representative images of DNA Fibers 24hr ±Hydroxurea in U2OS cells 72hr post-transfection with the indicated siRNAs (Left). Quantification of IdU only labeled fibers, representing stalled replication, after indicated times of HU exposure 72hr post-transfection with indicated the siRNAs (Top Right). Quantification of CldU only labeled fibers, representing new origins of replication, after indicated times of HU exposure 72hr post-transfection with indicated the siRNAs. Bars indicate mean and SEM from 3 independent experiments. * indicates p= <0.05; ** indicates p <0.01.

Figure 5: Sec8 modulates accumulation and activity of DNA-damage associated histone-modifiers (A) SGA derived correlation network centered on the yeast exocyst component Sec3 as derived from the Drygin similarity matrix. Node length corresponds to r value. Sec15 r = 0.282, Sec10 r = 0.278, Exo70 r = 0.23, HPA2 r =0.221 **(B)** Immunoblots from whole-cell lysates with indicated antibodies in U2OS cells after exposure to 5 Gy irradiation and incubation for indicated time points 72hr post-transfection with the indicated siRNAs. Results shown are representative of 3

independent experiments. **(C)** qRT-PCR analysis of relative ATF2 mRNA expression in U2OS cells 72hr post-transfection with the indicated siRNAs. Experiment performed in triplicate. **(D)** Immunoblots from whole-cell lysates with indicated antibodies in U2OS cells 72hr post-transfection with the indicated siRNAs. **(E)** Representative images of nuclear ATF2 in U2OS cells transfected with indicated siRNAs (Left). Image-based quantification of ATF2 nuclear intensity with ImageJ using a DAPI mask and mean intensity. Results shown represent the mean of 2 independent experiments (Right). MM 34.57 ± 0.9943 N=84; Sec8 49.68 ± 1.718 N=77, *** p= <0.0001. **(F,G)** Accumulation of the indicated proteins was evaluated as in B. Results shown are representative of 3 independent experiments. **(H)** qRT-PCR analysis of relative RNF20 expression in U2OS cells 72hr post-transfection with the indicated siRNAs. Experiment performed in triplicate. **(I)** Representative images of Rad51 foci in U2OS cells with 0 Gy or 4hr post 5 Gy irradiation 72hr post-transfection with the indicated siRNAs (Left). Image-based quantification of Rad51 foci is shown on the right. Cells with >8 foci were scored as positive. MM 16.10 ± 0.4403 N=124; Sec8 19.84 ± 0.6516 N=116, **** indicates p= <0.0001.

Figure 6: Schematic depicting suggested spatial and temporal regulation of histone modifying proteins driven by Sec8 and the exocyst complex.

Materials and Methods

Cell Culture

U2OS (from ATCC) cells were cultured in McCoy's 5A medium supplemented with 10% FBS. HBEC3 KT cells were cultured in KSFM (Invitrogen). MCF7A DR-GFP cells were cultured in DMEM supplemented with 10% FBS and 10 ng/ml Puromycin. U2OS GFP-LC3 were maintained in DMEM supplemented with 10% FBS and 1 mg/ml G418 and 5 mg/ml Blasticidin.

P53 siRNA screen

siRNA pools (4xsiRNAs) targeting a single CRC candidate gene[87] were obtained from the Qiagen Human Whole genome siRNA library (Version 1.0). HCT116 or RKO cells were transiently transfected with the pp53-TA-Luc reporter (Clontech), SV40-RL reporter, and siRNAs using Effectene (Qiagen). A final concentration of 33nM siRNA was used to transfect 10,000 cells plated in 96 well plates. Experiments were performed in triplicate. Firefly and *Renilla* luciferase activities were measured after 36 hours using the Dual Luciferase Reporter assay system (Promega). Normalized p53 activity was calculated as the ratio of firelfly to *Renilla* luciferase.

Yeast Two-Hybrid Screen and Mass Spec Analysis

The coding sequence for full-length human SEC3, SEC5, SEC6, SEC8, SEC10, EXO84, and EXO70 was cloned into pB27 as a C-terminal fusion to LexA and used as a bait to screen at saturation a high-complexity random-primed human placenta cDNA library as

previously described[67]. Using the raw data, an interaction map was generated from all potential interactions with a confidence score of "D" or higher in the screen (confidence score is detailed in[69]). Proteins were manually assigned a function in the DNA damage response by a curated literature search.

Immunoprecipitation and Immunoblotting

U2OS cells and HBEC 3KT cells were seeded onto 10cm dishes and allowed to grow to 100% confluency for immunoprecipitation or seeded on 35mm dishes for transfection and immunoblot. For IP, cell cultures were washed with cold PBS and lysed on ice for 10 min. in 20 mM Tris-HCl pH 7.4, 137mM NaCl, 10% Glycerol, 1% Triton X-100, 0.5% sodium deoxycholate, 10mM $MgCl_2$, 2mM EGTA plus protease and phosphatase inhibitors (Roche EDTA-free protease inhibitor cocktail, 1mM PMSF, 50mM NaF, 1mM $NaVO_4$, 80mM b-glycerosphosphate), then dounced 15 times. Lysates were then centrifuged at 20,000 X g for 10 min at 4°C. Soluble fractions were collected and protein concentration was assessed by Precision Red Advanced Protein Assay (Cytoskeleton, Inc). Protein A/G beads and mouse HA antibody (Santa Cruz) were used to clear non-specific interactions for 1hr at 4°C. Cleared lysates were incubated with indicated antibodies (1 mg ab: 200 mg lysate) coupled to protein A/G beads for 1hr at 4°C. Beads were then washed with lysis buffer three times followed by elution of protein in 2x SDS sample buffer.

For overexpression/co-immunoprecipitation, 293T cells were seeded at $2x10^5$ cells onto 35mm dishes 24hr before transfection. 2 mg total DNA was transfected with Fugene 6 at

a ratio of 1:3 in Opti-MEM. 72hr post-transfection, cells were lysed and processed as described above..

Immunofluorescence

For colocalization studies, cells were cultured on coverslips, fixed and permeablized with methanol at -20°C for 1 minute, blocked with 5% BSA in 0.1% TBS-Triton X-100 for 20 minutes at 37°C, washed in .1% TBS-T, and sequentially incubated with Sec8 (10C2) primary and Donkey Anti-Mouse Rhodamine (Jackson ImmunoResearch Laboratories, inc.) secondary antibodies and 53bp1 (Bethyl) primary and Alex-488 Donkey Anti-Rabbit (Invitrogen) secondary antibodies for 1 hour each at 37°C. Nuclei were counter-stained with DAPI (Vectashield Mounting media, Vector Laboratories). Slides were imaged using the Leica TCS SP5 confocal microscope (Leica Micro-systems, CMS GMBH) with custom software (Leica Micro-systems LAS AF) using a sequential 3-channel scan. All images were captured using the same electronic settings. Images were imported to ImageJ (http://rsb.info.nih.gov) using the LOCI Bio-formats plug-in (University of Wisconsin, Madison).

For analysis of DDR foci, siRNA transfected cells were cultured in chamber slides, fixed in 2% paraformaldehyde for 15 min, washed in phosphate-buffered saline (PBS), permeabilized for 5 min on ice in 0.2% Triton X-100, and blocked in PBS with 1% bovine serum albumin. Immunostaining protocols were as previously described[114,115]. Epifluorescence images were captured using a Zeiss Axioskop 2 mot epifluorescence microscope equipped with a charge-coupled device camera and ISIS software

(Metasystems, Altlussheim, Germany). All results shown are from three independent experiments.

For ATF2 nuclear analysis**,** cells were seeded onto 2-well glass chamber slides and were subsequently transfected as previously described with control or Sec8 siRNA. 72 hours post-transfection cells were fixed and stained as previously described and Epifluorescence images were captured by using a Zeiss Axioskop 2 mot epifluorescence microscope equipped with a charge-coupled device camera and ISIS software (Metasystems, Altlussheim, Germany). Images were blinded and scored by calculating mean nuclear intensity using DAPI as a mask in ImageJ. Data represents at least 2 independent experiments with N>75.

GFP-LC3 quantitation.

Total GFP fluorescence per cell was measured by flow cytometry of at least 10,000 events per condition on a BD FACSCalibur using CellQuest and FlowJo software. For visualization of GFP-LC3 positive punctae, cells were cultured on glass coverslips, rinsed in PBS, fixed with 3.7% paraformaldehyde, permeabilized with cold acetone, and mounted with Vectashield containing DAPI. Images were acquired using a Zeiss Axioplan 2E microscope and Hamamatsu monochrome digital camera with OpenLab software.

Cell Cycle Analysis

U2OS cells were harvested after irradiation (^{137}Cs Mark 1 irradiator, JL Shepherd &

Associates) and fixed in 80% ethanol at 4°C. Cells were centrifuged and washed in 1% BSA, 0.1% Tween-20 in PBS, and were either labeled with Mouse anti-Phospho-MPM2 for 3hr at RT, pelleted and labeled with Goat anti-Mouse Alexa 488 for 30 min and/or resuspended in PI/RNAase staining buffer (BD Pharmingen) for 30 minutes at 37°C. 20,000 events were analyzed on a BD FACSCalibur using CellQuest and FlowJo software.

DNA Fragmentation Analysis

Neutral comet assays were performed with the CometAssay kit (Trevigen) according to manufacturer's instructions. 72 hours post-transfection, cells were irradiated with the indicated doses and incubated for 30 min. Cultures were then trypsinized and diluted to $1x10^5$ cells/ml in PBS, mixed with molten LMAgarose at a 1:10 ratio, and spotted on glass slides. After solidification, slides were immersed in lysis solution at 4°C for 30 min, and equilibrated in chilled neutral electrophoresis buffer for 30 min. Electrophoresis was performed in neutral electrophoresis buffer for 20 min with a electric field of 1 V/cm. Slides were further treated with DNA Precipitation Solution followed by 70% ethanol for 30 min each at room temperature. After air-drying, cells were stained with SYBR Green (1 mg/ml). Comet images were captured with an epifluorescence microscope (Zeiss Axioplan 2E). Comet tails were measured according to pixel length with ImageJ.

DR-GFP Assay

MCF7-DR GFP stable cells were derived as previously described[116], transfected with indicated siRNAs and assayed 72 hr post-transfection. To measure the repair of I-*Sce*I-generated DSBs, the I-*Sce*I plasmid was mixed with Lipofectamine 2000 at a ratio of 1:2.

The percentage of cells that were GFP-positive was quantitated with flow cytometric analysis on a Becton Dickinson FACScan 48 hr post- I-*Sce*I transfection.

DNA Fiber Assay

Fiber assays were performed as previously described[117]. Briefly, exponentially growing cells were pulsed with 50 mM 5-iododeoxyuridine (IdU) for 20 min, washed three times with phosphate-buffered saline (PBS), treated with 2 mM hydroxyurea (HU) for the indicated intervals, washed three times with PBS, incubated in fresh medium containing with 50 mM5-chlorodeoxyuridine (CldU) for 20 min, and then washed three times in PBS. DNA fiber spreads were produced with a modified procedure described previously[101]. IdU and CldU-labeled cells were mixed with unlabeled cells in a ratio of 1:10. 2 ml cell suspensions were then dropped onto a glass slide and mixed with a 20 ml hypotonic lysis solution (10 mM Tris-HCl, pH 7.4, 2.5 mM MgCl2, 1 mM phenylmethylsulfonyl fluoride [PMSF], and 0.5% Nonidet P-40) for 8 min. Air-dried slides were fixed, washed with 1x PBS, blocked with 5% bovine serum albumin (BSA) for 15 min, and incubated with primary antibodies against IdU and CldU (rat monoclonal antibody [MAb] anti-IdU [1:150 dilution; Abcam] and mouse MAb anti-CldU [1:150 dilution; BD]) and secondary antibodies (anti-rat Alexa 488 [1:150 dilution] and anti-mouse Alexa 568 [1:200 dilution]) for 1 h each. Slides were washed with 1x PBS with 0.1% Triton X-100 and mounted with Vectashield mounting medium without DAPI.

Metaphase Spread Analysis

Control or Sec8 siRNA transfected U2OS cells were irradiated with 1 Gy of ioninizing radiation, incubated for 2 hr and then exposed to Colcemid (Sigma–Aldrich) (0.1 lg per ml). After 3 hr Colcemid treatment, cells were harvested. Metaphase spreads were prepared and analyzed as described previously[118,119]. 50 metaphases were scored/sample, and each sample was analyzed three times. Mean and standard deviation is from three independent experiments.

Clonogenic Survival Assay

Control or Sec8 siRNA transfected U2OS cells were re-plated into 60-mm dishes in 5.0 ml of medium, incubated for 7 hr and subsequently exposed to graded doses (0, 2, 4, 6, 10 Gy) of ionizing radiation (Cs^{137}, dose rate 1 Gy per min). Cells were incubated for 12 days, and fixed in methanol:acetic acid (3:1) prior to staining with crystal violet. Only colonies containing >50 cells were counted. Survival fractions were reported as a mean of three independent experiments.

qRT-PCR

Control or Sec8 siRNA transfected cells were collected and RNA was extracted using a Qiagen RNAeasy (#74104) kit. cDNA was made using 100 ng of RNA for all samples using iScript reagents from BioRad. ATF2 or RNF20 TaqMan probes (Applied Biosystems) were used for real-time analysis on a Roche LightCycler. Expression levels were calculated comparing the CT values of target genes to b-Actin (used as an internal control) and the fold change by comparing the CT values of untreated versus treated

samples. The experiment was done in triplicate.

siRNA Sequences

siGenome pools were purchased from Dharmacon for the following genes: SEC8 (EXOC4), SEC3, SEC5, SEC6, SEC10, SEC15, EXO70, TP53BP1, TP53, ULK1, BECN1, HUWE1, and UBR5. Control siRNA was the Non-Targeting Pool #2 (Cat #: D-001206-14-05). EXO84 was custom designed with the following sequence: 5'-GCCACUAAACAUCGCAACUdTdT-3'

Plasmids and Reagents

Myc-Sec8[21], Flag-53bp1[120] pCMV-I-SceI[121] were described previously. Aphidicolin was diluted in DMSO at a stock concentration of 2 mg/ml. Hydroxyurea was diluted in DMSO. CPT was diluted in PBS.

Antibodies

Mouse anti-HA (sc-7392) and Rabbit anti-Myc (sc-789) were purchased from Santa Cruz Biotechnology, Inc. Rabbit anti-Flag (#F2555) Mouse anti-βActin (#A1978), and Mouse anti-Flag (#F1804) were purchased from Sigma-Aldrich, Inc. Rabbit anti-53bp1 (A300-272A) was purchased from Bethyl Laboratories. Mouse anti-γH2AX (#16-193), Mouse anti-Phospho-MPM2 (#05-368), and Rabbit anti-Tip60 (#07-038) were purchased from Millipore. Mouse Sec8 was provided by Charles Yeaman[122-124]. Rabbit anti-ATF2 (#9226), Rabbit anti-H2B (#8135), Rabbit anti-H2BK120ub (#5546), Rabbit anti-H3K4me3 (#9751), and Rabbit anti-H3K79me3 (#4260) were purchased from Cell Signaling Technology. Rabbit anti-Phospho ATF2 (S490/498) (#PAB9605) was

purchased from Abnova. Mouse anti-Rad51(#ab213) was purchased from Abcam.

Sec3 Network Representation

Network visualization of SGA genetic correlations with Sec3 was downloaded from DRYGIN database (http://drygin.ccbr.utoronto.ca/).

Image Editing

Images were edited and enhanced for visual purposed using ImageJ, Photoshop, and Microsoft PowerPoint. Quantification was performed on unaltered images.

Statistical Analysis

P values were calculated by two-tailed *t*-test. All data were analyzed using Graphpad Prism 5 & 6.

Figure 1:

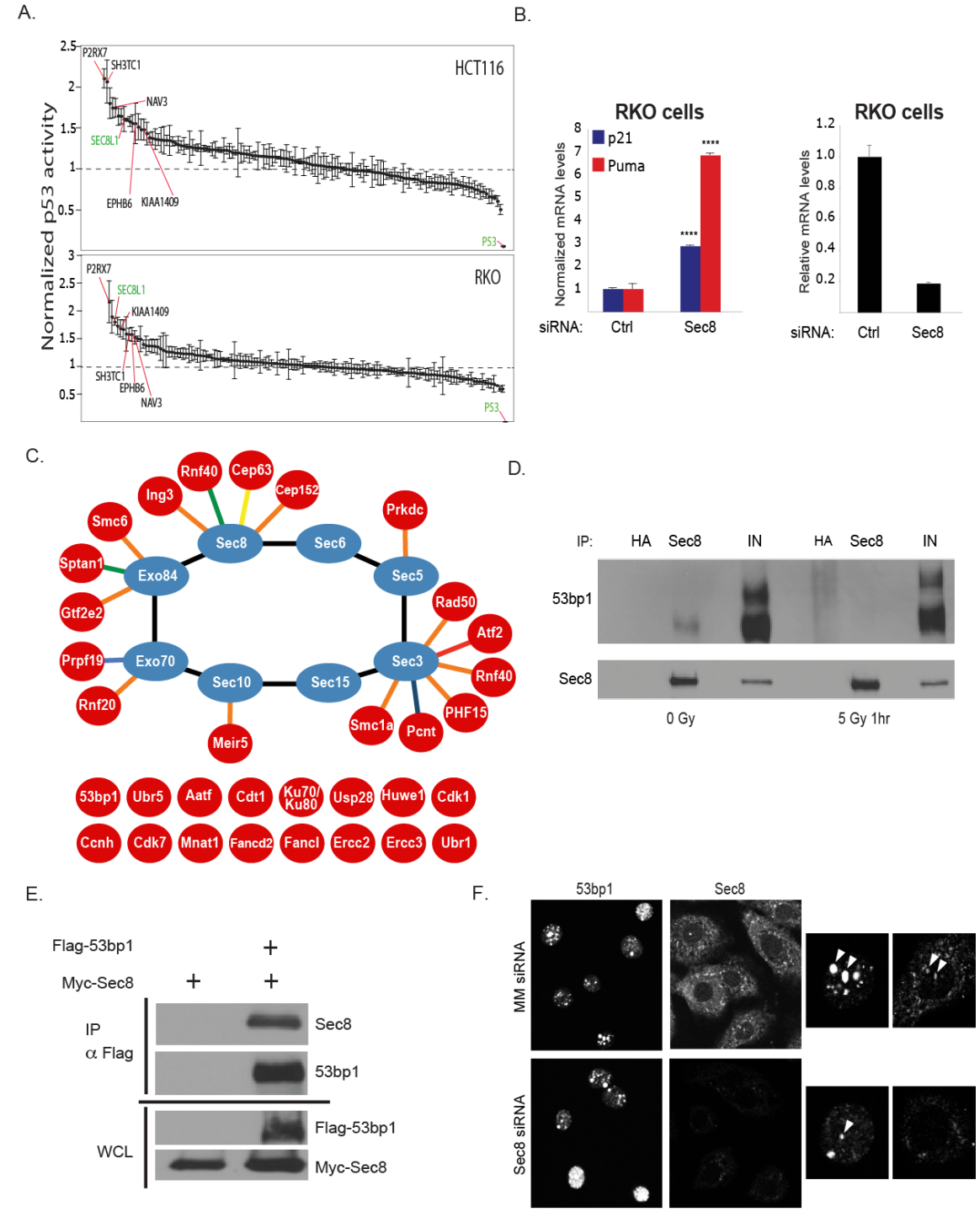
A.
HCT116
RKO
Normalized p53 activity
P2RX7
SH3TC1
NAV3
SEC8L1
EPHB6
KIAA1409
P53
B.
RKO cells
p21
Puma
Normalized mRNA levels
siRNA:
Ctrl
Sec8
RKO cells
Relative mRNA levels
C.
Rnf40
Cep63
Cep152
Ing3
Smc6
Prkdc
Sec8
Sec6
Sptan1
Exo84
Sec5
Rad50
Gtf2e2
Atf2
Prpf19
Exo70
Sec3
Rnf40
Sec10
Sec15
Rnf20
PHF15
Smc1a
Pcnt
Meir5
53bp1
Ubr5
Aatf
Cdt1
Ku70/Ku80
Usp28
Huwe1
Cdk1
Ccnh
Cdk7
Mnat1
Fancd2
Fancl
Ercc2
Ercc3
Ubr1
D.
IP:
HA
Sec8
IN
53bp1
Sec8
0 Gy
5 Gy 1hr
E.
Flag-53bp1
Myc-Sec8
IP
α Flag
WCL
F.
53bp1
Sec8
MM siRNA
Sec8 siRNA

Figure 2:

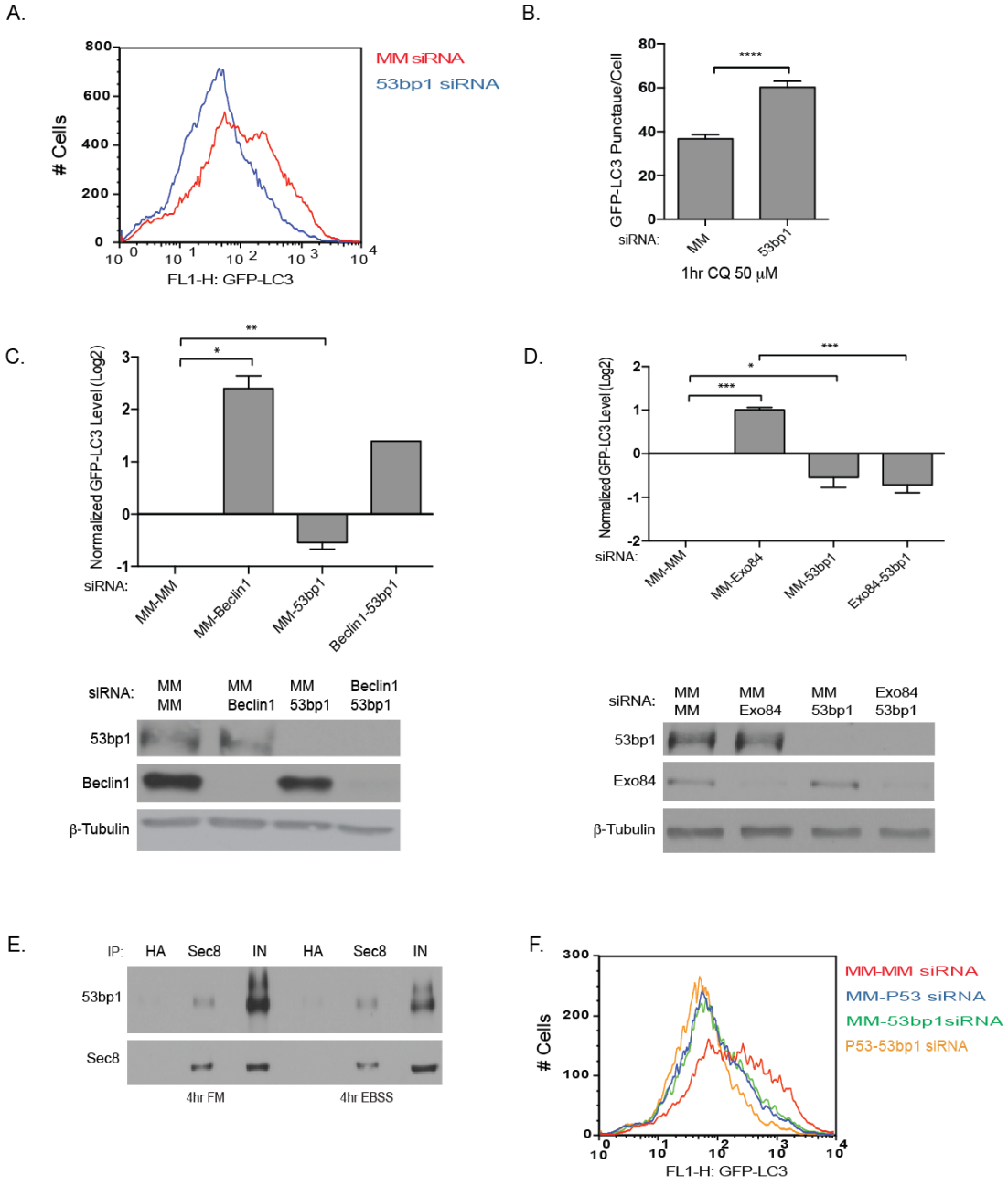
A.
MM siRNA
53bp1 siRNA
Cells
FL1-H: GFP-LC3
B.
GFP-LC3 Punctaue/Cell
siRNA:
MM
53bp1
1hr CQ 50 μM
C.
Normalized GFP-LC3 Level (Log2)
siRNA:
MM-MM
MM-Beclin1
MM-53bp1
Beclin1-53bp1
siRNA: MM MM MM Beclin1 MM 53bp1 Beclin1 53bp1
53bp1
Beclin1
β-Tubulin
D.
Normalized GFP-LC3 Level (Log2)
siRNA:
MM-MM
MM-Exo84
MM-53bp1
Exo84-53bp1
siRNA: MM MM MM Exo84 MM 53bp1 Exo84 53bp1
53bp1
Exo84
β-Tubulin
E.
IP: HA Sec8 IN HA Sec8 IN
53bp1
Sec8
4hr FM
4hr EBSS
F.
Cells
MM-MM siRNA
MM-P53 siRNA
MM-53bp1siRNA
P53-53bp1 siRNA
FL1-H: GFP-LC3

Figure 3:

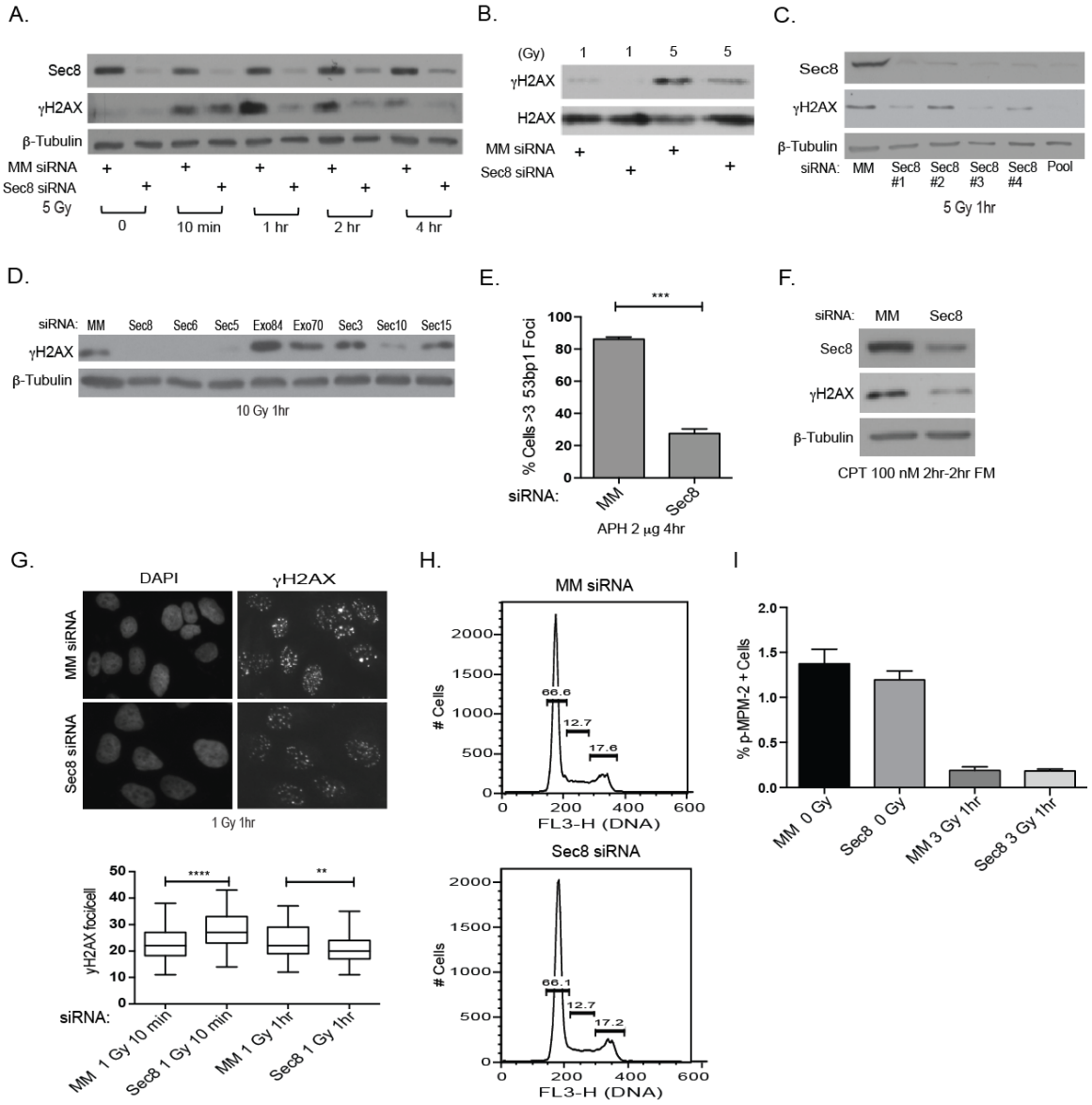
A.
Sec8
γH2AX
β-Tubulin
MM siRNA
Sec8 siRNA
5 Gy
0
10 min
1 hr
2 hr
4 hr
B.
(Gy) 1 1 5 5
γH2AX
H2AX
MM siRNA
Sec8 siRNA
C.
Sec8
γH2AX
β-Tubulin
siRNA: MM Sec8 #1 Sec8 #2 Sec8 #3 Sec8 #4 Pool
5 Gy 1hr
D.
siRNA: MM Sec8 Sec6 Sec5 Exo84 Exo70 Sec3 Sec10 Sec15
γH2AX
β-Tubulin
10 Gy 1hr
E.
% Cells >3 53bp1 Foci
siRNA: MM Sec8
APH 2 μg 4hr
F.
siRNA: MM Sec8
Sec8
γH2AX
β-Tubulin
CPT 100 nM 2hr-2hr FM
G.
DAPI
γH2AX
MM siRNA
Sec8 siRNA
1 Gy 1hr
γH2AX foci/cell
siRNA:
MM 1 Gy 10 min
Sec8 1 Gy 10 min
MM 1 Gy 1hr
Sec8 1 Gy 1hr
H.
MM siRNA
Cells
66.6
12.7
17.6
FL3-H (DNA)
Sec8 siRNA
66.1
12.7
17.2
I
% p-MPM-2 + Cells
MM 0 Gy
Sec8 0 Gy
MM 3 Gy 1hr
Sec8 3 Gy 1hr

Figure 4:

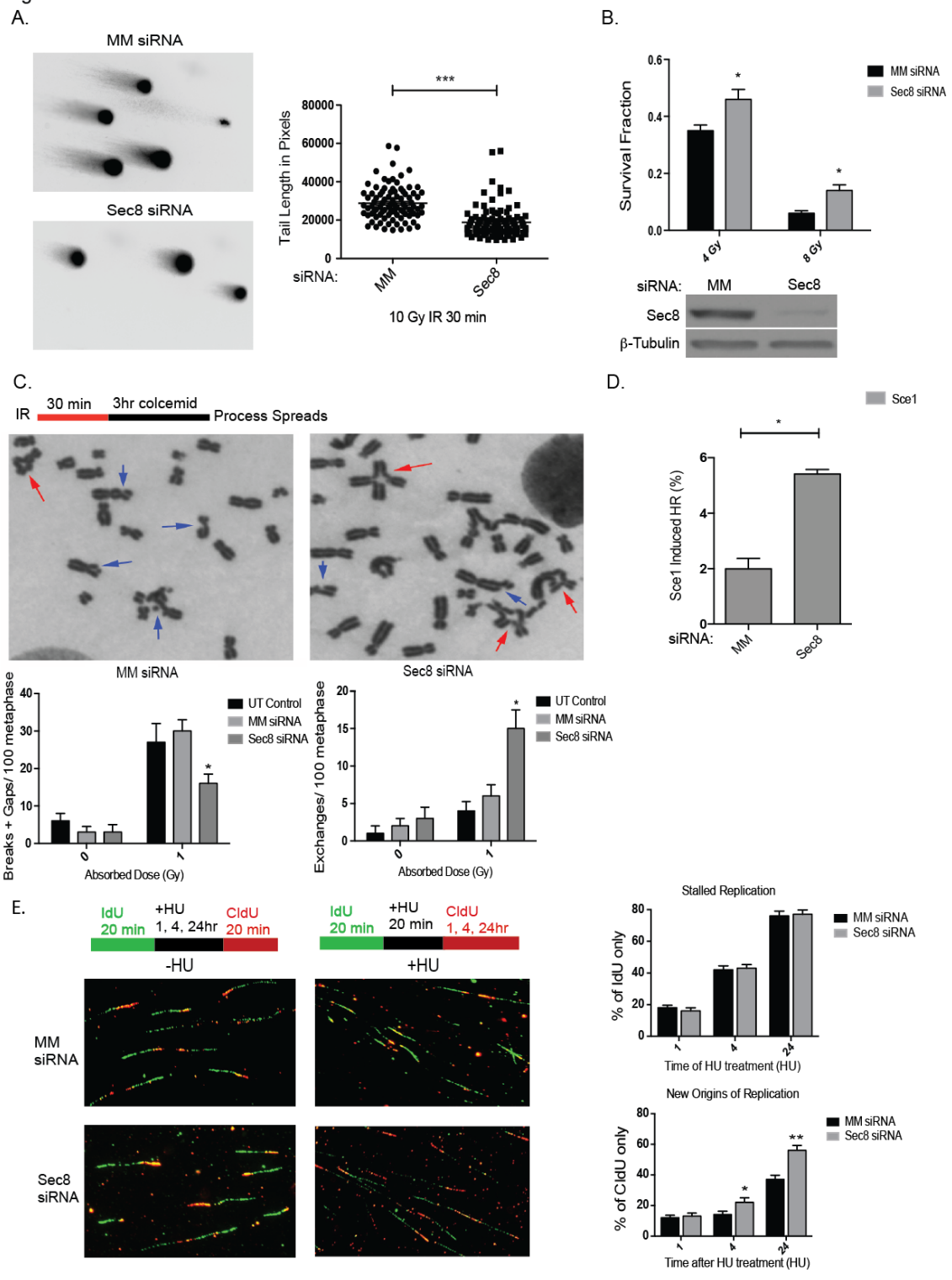
A.
MM siRNA
Sec8 siRNA
***
Tail Length in Pixels
80000
60000
40000
20000
0
siRNA:
MM
Sec8
10 Gy IR 30 min
B.
MM siRNA
Sec8 siRNA
Survival Fraction
0.6
0.4
0.2
0.0
*
*
4 Gy
8 Gy
siRNA:
MM
Sec8
Sec8
β-Tubulin
C.
IR
30 min
3hr colcemid
Process Spreads
MM siRNA
Sec8 siRNA
Breaks + Gaps/ 100 metaphase
UT Control
MM siRNA
Sec8 siRNA
Absorbed Dose (Gy)
Exchanges/ 100 metaphase
Absorbed Dose (Gy)
D.
Sce1
Sce1 Induced HR (%)
siRNA:
MM
Sec8
E.
IdU
20 min
+HU
1, 4, 24hr
CldU
20 min
-HU
+HU
MM
siRNA
Sec8
siRNA
Stalled Replication
% of IdU only
Time of HU treatment (HU)
New Origins of Replication
% of CldU only
Time after HU treatment (HU)

Figure 5:

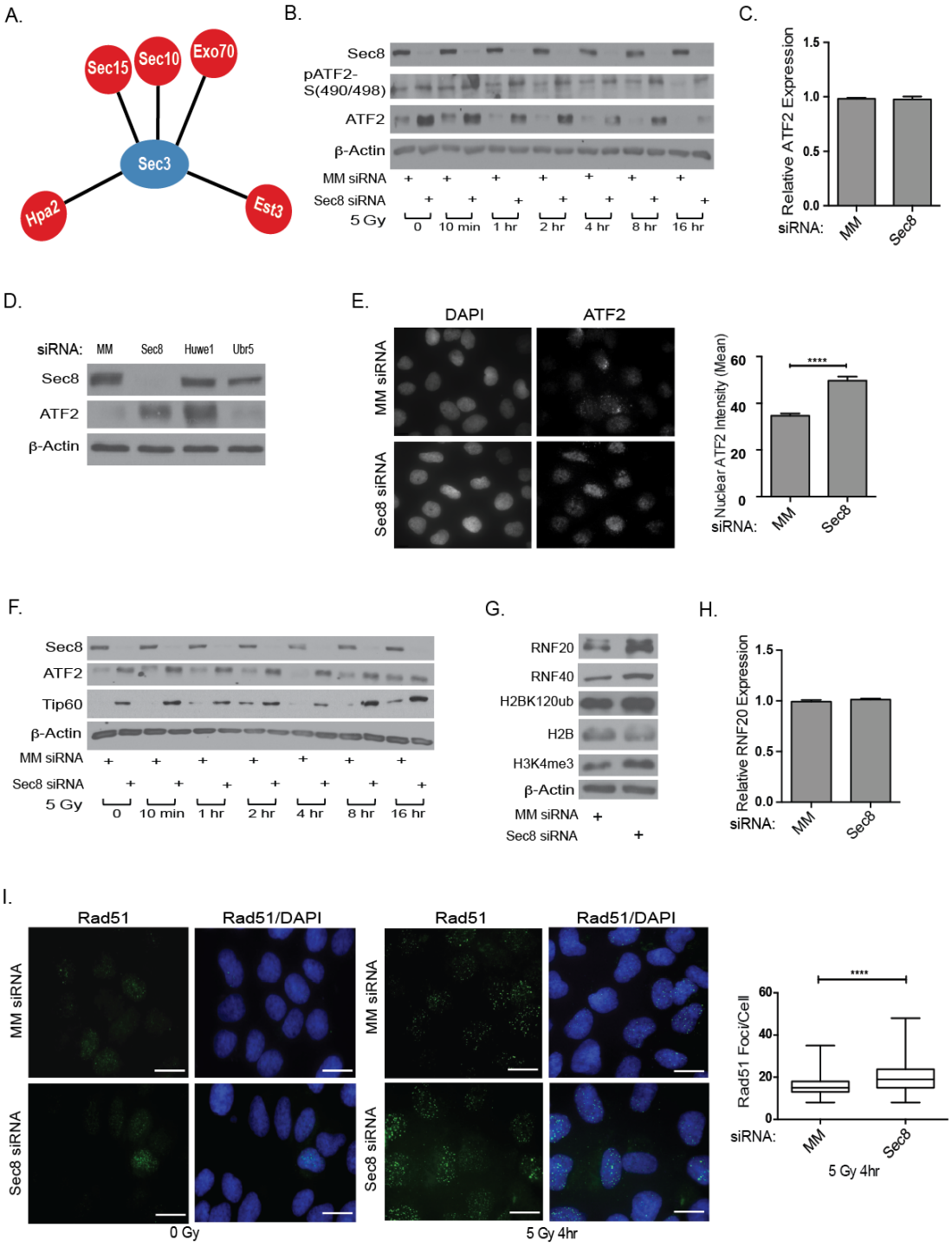
A.
Sec15
Sec10
Exo70
Sec3
Hpa2
Est3
B.
Sec8
pATF2-S(490/498)
ATF2
β-Actin
MM siRNA
Sec8 siRNA
5 Gy
0
10 min
1 hr
2 hr
4 hr
8 hr
16 hr
C.
Relative ATF2 Expression
siRNA:
MM
Sec8
D.
siRNA:
MM
Sec8
Huwe1
Ubr5
Sec8
ATF2
β-Actin
E.
DAPI
ATF2
MM siRNA
Sec8 siRNA
Nuclear ATF2 Intensity (Mean)
****
siRNA:
MM
Sec8
F.
Sec8
ATF2
Tip60
β-Actin
MM siRNA
Sec8 siRNA
5 Gy
0
10 min
1 hr
2 hr
4 hr
8 hr
16 hr
G.
RNF20
RNF40
H2BK120ub
H2B
H3K4me3
β-Actin
MM siRNA
Sec8 siRNA
H.
Relative RNF20 Expression
siRNA:
MM
Sec8
I.
Rad51
Rad51/DAPI
MM siRNA
Sec8 siRNA
0 Gy
5 Gy 4hr
Rad51 Foci/Cell
****
siRNA:
MM
Sec8
5 Gy 4hr

Figure 6:

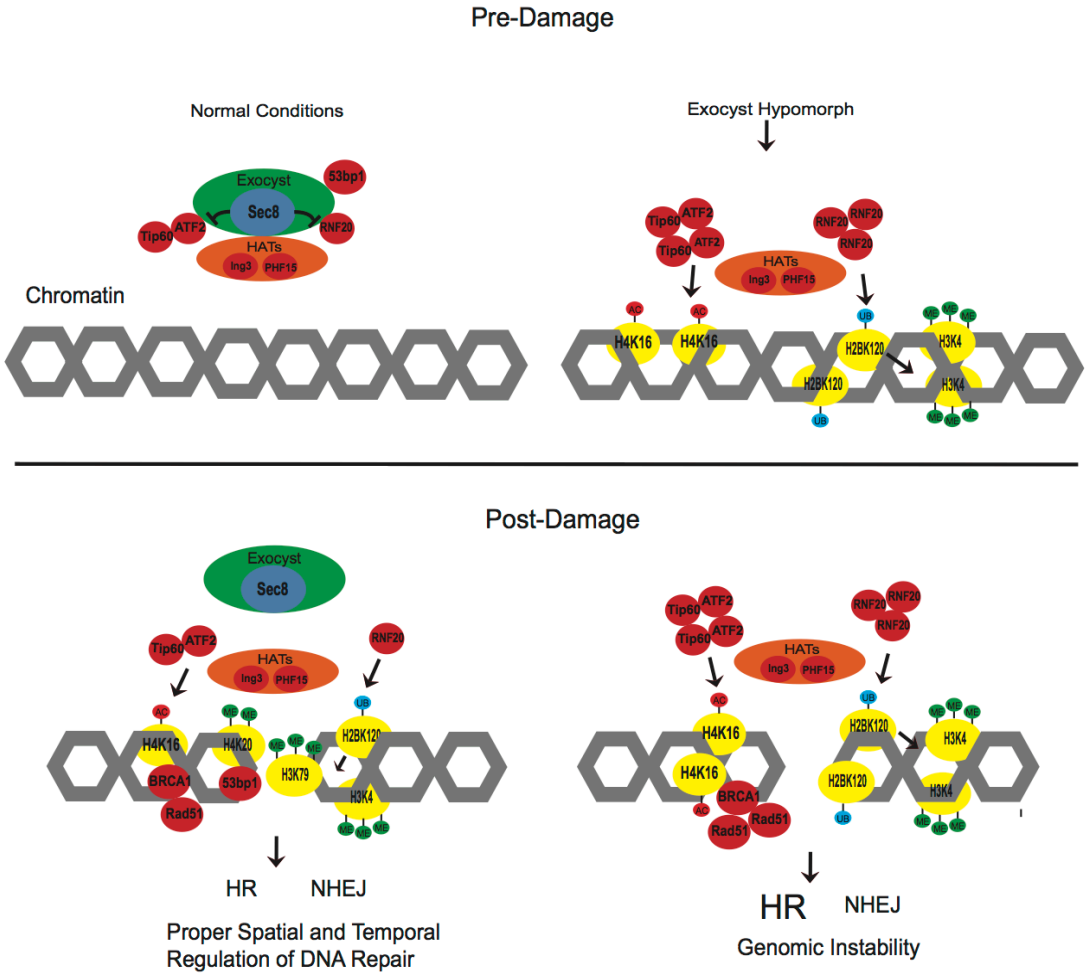
Pre-Damage
Normal Conditions
Exocyst Hypomorph
Exocyst
Sec8
53bp1
Tip60
ATF2
RNF20
HATs
Ing3
PHF15
Chromatin
H4K16
H2BK120
H3K4
Post-Damage
H4K20
H3K79
BRCA1
Rad51
HR
NHEJ
Proper Spatial and Temporal
Regulation of DNA Repair
Genomic Instability

CHAPTER FOUR
Future Directions and Concluding Remarks

TBK1-Exocyst-AKT Network in Cancer

The exocyst complex, as a spatial and temporal signaling platform, is involved in many cellular processes. Our investigation of how the exocyst complex is altered in cancer cell biology has yielded insight into additional roles for the exocyst. Our data has given mechanistic insight into the importance of the exocyst complex in driving aberrant AKT activation mediated by RalB and TBK1. This study has solidified TBK1 as a potential therapeutic target in cancer and uncovered a previously unknown connection between innate immunity and the AKT pro-survival pathway. Expansion of pre-clinical models of TBK1 inhibition is necessary in the development of TBK1 inhibitors and determination of their utility as a cancer therapeutic.

A major unanswered question that remains is: What is the mechanism that determines TBK1 dependency? Our lung cancer panel is an excellent platform to examine commonalities between cell lines that are sensitive to TBK1 inhibition and cell lines that are insensitive to TBK1 inhibition. Utilizing the mutation status and microarray data of mRNA expression levels will allow us to find potential biomarkers that predict sensitivity. This will allow us to test whether there is a functional dependence on these alterations that provides a mechanistic basis for TBK1 sensitivity in a subset of non-small cell lung cancers. We still do not fully understand the mechanistic contribution of TBK1 to the AKT pathway, and there may be additional functions for TBK1 and the exocyst in

the AKT axis that contributes to oncogenesis. This can be studied through biochemical assays that seek to identify additional TBK1-exocyst interacting proteins. One method to accomplish this would be to immunoprecipate TBK1 and perform mass spectroscopy analysis to determine additional interacting partners that could be substrates of TBK1 that are aberrantly regulated in cancer. This would allow for strengthening of TBK1 pre-clinical model, and further understanding of TBK1 driven cancer cell survival.

Exocyst in DNA Repair

This study found an unexpected connection between DNA repair proteins and the exocyst complex. Given that genomic instability is associated with cancer, we have uncovered an additional role for the exocyst complex in suppressing tumorigenic activity by regulating histone modifications that are important in directing repair proteins. We have hints, with the interaction with 53bp1, that localization of proteins may also be another layer of exocyst regulation. Thus, like previously characterized functions of the exocyst, it seems likely that spatial regulation of interacting proteins mediated by the exocyst is important in normal protein function.

There are several outstanding questions that warrant further investigation. Although, we do have evidence to suggest that histone modifications alter repair choice, we still do not have a firm grasp of how depletion of Sec8 results in elevated protein levels of histone modifiers ATF2 and RNF20. Depletion of Huwe1, an E3 ligase that functions in DNA repair, upregulated ATF2, which suggests that regulation of Huwe1, might be facilitated

by exocyst interaction. Direct biochemical evidence is needed to further expound on this regulation. One way to test this would be to immunoprecipitate Sec8 and probe for Huwe1 by western blot to validate the interaction. Additionally, an examination of Huwe1 under Sec8 depleted conditions would allow us to determine whether depletion of Sec8 lowers the protein levels of this E3 ligase that may contribute to the post-translational upregulation of ATF2 and RNF20/RNF40.

An additional question not addressed is whether the exocyst complex as a whole contributes to proper maintenance of DNA repair, such that can be explained by Sec8 depletion, or if there are specific subunits that have specific effects in regulating DNA repair. Our previous observations suggest divergence in respect to alteration of γH2AX in response to irradiation with single subunit depletion. Therefore a careful examination of single subunit exocyst depletion with siRNAs would enable us to understand exocyst contribution to DNA repair, particularly in experiments such as colony formation, comet assay, metaphase spreads, and Rad51 foci which would measure recombination and repair choice.

Furthermore, DNA repair consists of several pathways, but we only examined the response to irradiation and replication-coupled DNA damage. We do not yet know whether the exocyst complex is involved in other types of repair such as base-excision repair or inter-strand crosslink repair. Therefore, a study utilizing reagents to elicit these types of damage such as Mitomycin C or ultraviolet light under Sec8 depleted conditions

would be useful in further elaborating the role of the exocyst complex in this context. It seems likely that they exocyst complex may contribute to these types of repair as well, since there are proteins such as FANCD2, ERCC2, and ERCC3 that are involved in these pathways that are predicted to interact with the exocyst.

Moreover, we do not fully understand the contribution of Sec8 to oncogenesis. We have evidence that mutation and deletion of Sec8 is associated with colorectal cancer, but given the observation of increased IR survival, but increased genomic instability, it is not clear what the outcome of Sec8 depletion would be in regards to the process of oncogenesis. One way to address this would be to utilize mice that harbor conditional deletion of Sec8, which would allow for study of Sec8 contribution to oncogenesis after irradiation. Several questions could be answered using this model, such as whether Sec8 deletion is sufficient to drive oncogenesis and whether it is necessary to sensitize the mouse to tumorigenesis by introducing other oncogenic mutations such as p53 depletion or KRAS overexpression.

Exocyst Integration Into Broader Biological Contexts

This study provides the first integration of the exocyst complex into the DNA repair pathway, and adds to the growing number of biological contexts to which the exocyst participates in. Previous work from our lab has coupled nutrient sensing to the regulation of autophagy, a process that modulates nutrient availability, mediated by the exocyst complex. It is likely that there are additional levels of regulation between previously

characterized exocyst functions and the newly characterized role for the exocyst in DNA repair.

One such integration could be between cytokinesis and resolution of chromosome bridges, which can arise from incomplete segregation of chromosomes or unrepaired DSBs, that are a source of genomic instability[125,126]. One potential barrier to genomic instability by chromosome bridges is to delay abscission. This is mediated by the Aurora B kinase stability, which is necessary to stabilize mitotic kinesin-like protein 1 (Mklp1) to suppress furrow regression, which takes place at the midbody [125]. It has also been shown that DDR proteins, such as Rad50 can localize to chromosome bridges and the midbody, and in the case of Rad50 are necessary for chromosome bridge formation after DNA damage, which may represent a barrier to aberrant cytokinesis[127]. The exocyst also localizes to the midbody and is required for abscission. The function of exocyst involvement in abscission is thought to be primarily through delivery of secretory vesicles at the midbody that mark the site of abscission[14]. Our exocyst PPI predicts an interaction with Rad50, therefore, an additional level of integration may be the spatial regulation of DDR proteins to sites of chromosome bridges and the midbody in order to allow for proper resolution of missegregated chromosomes. This may also integrate with p53 as missegregated chromosomes cause a p53-dependent cell cycle delay that allows for repair and suppression of genomic instability[128], which may explain the upregulation of p53 targets we see upon Sec8 depletion in p53-positive cells. Thus, an additional level

of integration of the exocyst may be to facilitate proper localization and activation of DDR proteins to the midbody in order to suppress aberrant cytokinesis.

An additional level of integration worth considering is the coupling of the host defense response recognition of double-stranded DNA viruses and DDR proteins, which bind to DNA that has been damaged. In response to foreign DNA, cells have evolved a host defense response that results in upregulation of anti-viral proteins via interferon regulatory factor-3 (IRF-3)[129]. This response is mediated by TBK1, which is activated by transmembrane protein 173 (TMEM173, also known as STING). As previously discussed, TBK1 interacts with the exocyst and this interaction with the exocyst is critical for its function in the host defense response[22]. Although, much is known about the transcriptional activation of anti-viral genes in response to foreign cytosolic DNA, little is known on how cells initially recognize cytosolic DNA. Recent reports have implicated protein kinase, DNA-activated, catalytic polypeptide (PRKDC, also known as DNA-PK) as a bona fide sensor of foreign cytosolic DNA that activates the innate immune response[130]. PRKDC is activated in response to DNA damage and can phosphorylate γH2AX[98,131], strongly establishing PRKDC in the DNA damage response pathway. However, it was shown that the kinase activity of PRKDC was dispensable for innate immune response activation[130]. PRKDC also localizes with STING and TBK1, thus suggesting the necessity of a signaling platform to mediate the recognition and subsequent activation of the host defense response in the presence of foreign DNA. Our exocyst PPI predicts an interaction with PRKDC. Given that it has already been shown

that the exocyst, by way of TBK1 and STING, participates in signal transduction cascades in response to foreign DNA, a way to facilitate the initial recognition of foreign DNA and the downstream host defense response would be spatial regulation mediated by the exocyst, thus potentially adding another layer of integration.

Emerging evidence suggests proteins involved in primary ciliogenesis mediate regulation of the DNA damage response and suppression of genomic instability[132]. This is quite intriguing as it is well established that the exocyst complex localizes to the primary cilium[133,134]. Primary cilia are involved in many biological processes from renal structure to sensory of light[134,135]. Interestingly mutations in cilia and/or their related centrosome proteins produce a disease class labeled ciliopathies. Ciliopathies share a broad disease spectrum, but have commonalities in their clinical features such as microcephaly, growth delay or even perinatal lethality, and renal failure in the form of polycystic kidney disease (PKD)[135]. A related disease that shares some of the same clinical features as well as common mutations in centrosome and DDR proteins is called Seckel Syndrome. Mutations in ATR (Ataxia Telangiectasia and Rad3 related), a key kinase involved in DNA single-stranded break repair, have also been coupled to Seckel Syndrome[136]. ATR has also been shown to localize to the cilia of photoreceptors suggesting potential need for DDR proteins in maintenance of proper cilia[137]. Interestingly, depletion of the exocyst subunit Sec10 has been implicated as being pathogenic in the etiology of PKD in zebrafish. It was shown that Sec10 was necessary for the proper localization of polycystin-2 (PKD2), a protein involved in calcium transport and calcium signaling in

renal epithelial cells, whose mutations also cause PKD[138]. Of note, is the finding that Sec10 depletion resulted in a less severe phenotype than PKD2, which may suggest subunit specific contributions that facilitate localization of the PKD2, but that this is not completely necessary for PKD2 function. Mutations in replication licensing factor, CDT1 (chromatin licensing and DNA replication factor 1), have also been implicated in the etiology of a Seckel-like syndrome by impacting cilia formation[139]. Centrosome proteins, CEP152 (centrosomal protein 152kDa) and PCNT (Pericentrin), both which have mutations linked to Seckel syndrome have been implicated in DNA repair[140,141]. Cell lines deficient in both CEP152 and PCNT show altered cell-cycle dynamics, however, γH2AX foci in response to DNA damage was normal with PCNT mutation yet elevated with CEP152 mutation, suggesting potential divergence in function within this disease context. However, both showed increased genomic instability, which may be associated with their centrosome function[140,141]. Our exocyst PPI predicts an interaction with CDT1, CEP152, and PCNT. Interestingly, in a study that sought to uncover novel candidate genes involved in the etiology of Meckel-Gruber syndrome, a severe perinatal lethal ciliopathy with clinical features such as occipital encephalocele, dysplastic kidneys, and polydactyly, one such candidate identified was Sec8. This was uncovered by exome sequencing of consanguineous families with Meckel-Gruber syndrome[6]. Given that less severe forms of ciiliopathies result from dysregulation of proteins that potentially interact with the exocyst, it must be considered that Sec8 dysregulation could alter the function of all or some of these proteins resulting in the severe ciliopathy that is associated with Sec8 mutation. Although the exocyst and centrosome protein have been firmly established now

in the DNA repair pathway and proper cilia function, little is known on how DDR proteins function in ciliogenesis. Given that the exocyst links these two biological processes, it is worth considering that the modulation of the exocyst may be an excellent tool to further uncover the function of DDR proteins in the maintenance of cilia, ciliogenesis, and DNA damage.

In summary, this work has helped to further illuminate the relevance of the exocyst complex as a spatial and temporal signaling platform important in driving responses to diverse cellular events. I have identified an additional role for the exocyst complex as a regulator of histone modifications important in driving efficient DNA repair and suppression of genomic instability. This newly revealed regulation of DNA repair by the exocyst may provide additional insight into the emerging observations of DNA damage protein involvement in pathways not canonically associated DNA repair, such as cytokinesis, host defense response, and maintenance of cilia. It is my hope that this work can become the basis for others to further explore the contribution of the exocyst complex in normal cell biology and in disease settings.

BIBLIOGRAPHY

1. Novick, P., Field, C. & Schekman, R. Identification of 23 complementation groups required for post-translational events in the yeast secretory pathway. *Cell* **21,** 205–215 (1980).
2. TerBush, D. R., Maurice, T., Roth, D. & Novick, P. The Exocyst is a multiprotein complex required for exocytosis in Saccharomyces cerevisiae. *EMBO J.* **15,** 6483–6494 (1996).
3. Murthy, M., Garza, D., Scheller, R. H. & Schwarz, T. L. Mutations in the exocyst component Sec5 disrupt neuronal membrane traffic, but neurotransmitter release persists. *Neuron* **37,** 433–447 (2003).
4. Friedrich, G. A., Hildebrand, J. D. & Soriano, P. The secretory protein Sec8 is required for paraxial mesoderm formation in the mouse. *Dev. Biol.* **192,** 364–374 (1997).
5. Yamamoto, A. *et al.* Exocyst complex component Sec8: a presumed component in the progression of human oral squamous-cell carcinoma by secretion of matrix metalloproteinases. *J Cancer Res Clin Oncol* (2012). doi:10.1007/s00432-012-1356-2
6. Shaheen, R. *et al.* Genomic analysis of Meckel-Gruber syndrome in Arabs reveals marked genetic heterogeneity and novel candidate genes. *Eur. J. Hum. Genet.* (2012). doi:10.1038/ejhg.2012.254
7. Ashktorab, H. *et al.* Distinct Genetic Alterations in Colorectal Cancer. *PLoS ONE* **5,** e8879 (2010).
8. Hsu, S. C. *et al.* Subunit composition, protein interactions, and structures of

the mammalian brain sec6/8 complex and septin filaments. *Neuron* **20,** 1111–1122 (1998).

9. Jin, R. *et al.* Exo84 and Sec5 are competitive regulatory Sec6/8 effectors to the RalA GTPase. *EMBO J.* **24,** 2064–2074 (2005).

10. Yamashita, M. *et al.* Structural basis for the Rho- and phosphoinositide-dependent localization of the exocyst subunit Sec3. *Nat. Struct. Mol. Biol.* **17,** 180–186 (2010).

11. Kim, D.-H. *et al.* mTOR interacts with raptor to form a nutrient-sensitive complex that signals to the cell growth machinery. *Cell* **110,** 163–175 (2002).

12. Chan, E. Y. W., Kir, S. & Tooze, S. A. siRNA Screening of the Kinome Identifies ULK1 as a Multidomain Modulator of Autophagy. *Journal of Biological Chemistry* **282,** 25464–25474 (2007).

13. Bodemann, B. O. *et al.* RalB and the Exocyst Mediate the Cellular Starvation Response by Direct Activation of Autophagosome Assembly. *Cell* **144,** 253–267 (2011).

14. Gromley, A. *et al.* Centriolin anchoring of exocyst and SNARE complexes at the midbody is required for secretory-vesicle-mediated abscission. *Cell* **123,** 75–87 (2005).

15. Guo, W., Tamanoi, F. & Novick, P. Spatial regulation of the exocyst complex by Rho1 GTPase. *Nat. Cell Biol.* **3,** 353–360 (2001).

16. Zhang, X. *et al.* Cdc42 interacts with the exocyst and regulates polarized secretion. *J. Biol. Chem.* **276,** 46745–46750 (2001).

17. Liu, J. & Guo, W. The exocyst complex in exocytosis and cell migration.

Protoplasma **249,** 587–597 (2012).

18. Das, A. & Guo, W. Rabs and the exocyst in ciliogenesis, tubulogenesis and beyond. *Trends Cell Biol.* **21,** 383–386 (2011).

19. Hildebrandt, M. C. R. A. A. G. R. G. R. C. G. S. H. W. T. H. W. Z. A. C. H. Y. G. G. R. C.-J. H. B. H. I. C. R. G. V. B. H. A. J. V. M. O. S. F. L. R. R. H. H. O. I.-B. T. Y. G. W. L. E. J. S. B. S. M. L. T. B. S. L. I. D. S. J. S. A. S. N. J. O. M. A. S. S. C. A. R. K. H. R. I. L. A. N. C. S. H. D. R. M. J. G. S. A. D. D. A. L. C. G. N. K. L. P. E. A. A. A.-R. R. L. H. O. E. Y. H. P. L. S. W. J. S. R. S. C. J. E. G. K. V. J. A. J. S. G. N. P. N. S. L. A. S. E. O. F. *et al.* Exome Capture Reveals ZNF423 and CEP164 Mutations, Linking Renal Ciliopathies to DNA Damage Response Signaling. *Cell* **150,** 533–548 (2012).

20. Sjöblom, T. *et al.* The consensus coding sequences of human breast and colorectal cancers. *Science* **314,** 268–274 (2006).

21. Moskalenko, S. *et al.* The exocyst is a Ral effector complex. *Nat. Cell Biol.* **4,** 66–72 (2001).

22. Chien, Y. *et al.* RalB GTPase-Mediated Activation of the IκB Family Kinase TBK1 Couples Innate Immune Signaling to Tumor Cell Survival. *Cell* **127,** 157–170 (2006).

23. Issaq, S. H., Lim, K.-H. & Counter, C. M. Sec5 and Exo84 foster oncogenic ras-mediated tumorigenesis. *Mol. Cancer Res.* **8,** 223–231 (2010).

24. Fitzgerald, K. A. *et al.* IKKepsilon and TBK1 are essential components of the IRF3 signaling pathway. *Nat. Immunol.* **4,** 491–496 (2003).

25. Häcker, H. & Karin, M. Regulation and function of IKK and IKK-related

kinases. *Sci. STKE* **2006,** re13 (2006).

26. Kawai, T. & Akira, S. Signaling to NF-kappaB by Toll-like receptors. *Trends Mol Med* **13,** 460–469 (2007).

27. Chau, T.-L. *et al.* Are the IKKs and IKK-related kinases TBK1 and IKK-epsilon similarly activated? *Trends Biochem. Sci.* **33,** 171–180 (2008).

28. Hiscott, J. Convergence of the NF-kappaB and IRF pathways in the regulation of the innate antiviral response. *Cytokine Growth Factor Rev.* **18,** 483–490 (2007).

29. Bodemann, B. O. & White, M. A. Ral GTPases and cancer: linchpin support of the tumorigenic platform. *Nat. Rev. Cancer* **8,** 133–140 (2008).

30. Korherr, C. *et al.* Identification of proangiogenic genes and pathways by high-throughput functional genomics: TBK1 and the IRF3 pathway. *Proc. Natl. Acad. Sci. U.S.A.* **103,** 4240–4245 (2006).

31. Barbie, D. A. *et al.* Systematic RNA interference reveals that oncogenic KRAS-driven cancers require TBK1. *Nature* **462,** 108–112 (2009).

32. Sharma, S. *et al.* Triggering the interferon antiviral response through an IKK-related pathway. *Science* **300,** 1148–1151 (2003).

33. Downward, J. Targeting RAS signalling pathways in cancer therapy. *Nat. Rev. Cancer* **3,** 11–22 (2003).

34. Manning, B. D. & Cantley, L. C. AKT/PKB signaling: navigating downstream. *Cell* **129,** 1261–1274 (2007).

35. Mitin, N., Rossman, K. L. & Der, C. J. Signaling interplay in Ras superfamily function. *Curr. Biol.* **15,** R563–74 (2005).

36. Chien, Y. & White, M. A. RAL GTPases are linchpin modulators of human tumour-cell proliferation and survival. *EMBO Rep.* **4,** 800–806 (2003).

37. Alessi, D. R. *et al.* Characterization of a 3-phosphoinositide-dependent protein kinase which phosphorylates and activates protein kinase Balpha. *Curr. Biol.* **7,** 261–269 (1997).

38. Engelman, J. A. Targeting PI3K signalling in cancer: opportunities, challenges and limitations. *Nat. Rev. Cancer* **9,** 550–562 (2009).

39. Guertin, D. A. *et al.* Ablation in mice of the mTORC components raptor, rictor, or mLST8 reveals that mTORC2 is required for signaling to Akt-FOXO and PKCalpha, but not S6K1. *Dev. Cell* **11,** 859–871 (2006).

40. Jacinto, E. *et al.* SIN1/MIP1 maintains rictor-mTOR complex integrity and regulates Akt phosphorylation and substrate specificity. *Cell* **127,** 125–137 (2006).

41. Sarbassov, D. D., Guertin, D. A., Ali, S. M. & Sabatini, D. M. Phosphorylation and regulation of Akt/PKB by the rictor-mTOR complex. *Science* **307,** 1098–1101 (2005).

42. Shiota, C., Woo, J.-T., Lindner, J., Shelton, K. D. & Magnuson, M. A. Multiallelic disruption of the rictor gene in mice reveals that mTOR complex 2 is essential for fetal growth and viability. *Dev. Cell* **11,** 583–589 (2006).

43. Li, X. *et al.* Autophosphorylation of Akt at threonine 72 and serine 246. A potential mechanism of regulation of Akt kinase activity. *J. Biol. Chem.* **281,** 13837–13843 (2006).

44. Forbes, S. A. *et al.* COSMIC (the Catalogue of Somatic Mutations in

Cancer): a resource to investigate acquired mutations in human cancer. *Nucleic Acids Research* **38,** D652–7 (2010).

45. Bamborough, P. *et al.* 5-(1H-Benzimidazol-1-yl)-3-alkoxy-2-thiophenecarbonitriles as potent, selective, inhibitors of IKK-epsilon kinase. *Bioorg. Med. Chem. Lett.* **16,** 6236–6240 (2006).

46. Clark, K., Plater, L., Peggie, M. & Cohen, P. Use of the pharmacological inhibitor BX795 to study the regulation and physiological roles of TBK1 and IkappaB kinase epsilon: a distinct upstream kinase mediates Ser-172 phosphorylation and activation. *J. Biol. Chem.* **284,** 14136–14146 (2009).

47. Bain, J. *et al.* The selectivity of protein kinase inhibitors: a further update. *Biochem. J.* **408,** 297–315 (2007).

48. Sato, S. *et al.* Toll/IL-1 receptor domain-containing adaptor inducing IFN-beta (TRIF) associates with TNF receptor-associated factor 6 and TANK-binding kinase 1, and activates two distinct transcription factors, NF-kappa B and IFN-regulatory factor-3, in the Toll-like receptor signaling. *J. Immunol.* **171,** 4304–4310 (2003).

49. Yamamoto, M. *et al.* Role of adaptor TRIF in the MyD88-independent toll-like receptor signaling pathway. *Science* **301,** 640–643 (2003).

50. Perry, A. K., Chow, E. K., Goodnough, J. B., Yeh, W.-C. & Cheng, G. Differential requirement for TANK-binding kinase-1 in type I interferon responses to toll-like receptor activation and viral infection. *J. Exp. Med.* **199,** 1651–1658 (2004).

51. Singh, A. *et al.* A gene expression signature associated with ‘K-Ras

addiction' reveals regulators of EMT and tumor cell survival. *Cancer Cell* **15,** 489–500 (2009).

52. Hresko, R. C. & Mueckler, M. mTOR.RICTOR is the Ser473 kinase for Akt/protein kinase B in 3T3-L1 adipocytes. *J. Biol. Chem.* **280,** 40406–40416 (2005).

53. Grindstaff, K. K. *et al.* Sec6/8 complex is recruited to cell-cell contacts and specifies transport vesicle delivery to the basal-lateral membrane in epithelial cells. *Cell* **93,** 731–740 (1998).

54. Guo, W., Sacher, M., Barrowman, J., Ferro-Novick, S. & Novick, P. Protein complexes in transport vesicle targeting. *Trends Cell Biol.* **10,** 251–255 (2000).

55. Ishikawa, H. & Barber, G. N. STING is an endoplasmic reticulum adaptor that facilitates innate immune signalling. *Nature* **455,** 674–678 (2008).

56. Ishikawa, H., Ma, Z. & Barber, G. N. STING regulates intracellular DNA-mediated, type I interferon-dependent innate immunity. *Nature* **461,** 788–792 (2009).

57. Bozulic, L. & Hemmings, B. A. PIKKing on PKB: regulation of PKB activity by phosphorylation. *Curr. Opin. Cell Biol.* **21,** 256–261 (2009).

58. Ericson, K. *et al.* Genetic inactivation of AKT1, AKT2, and PDPK1 in human colorectal cancer cells clarifies their roles in tumor growth regulation. *Proc. Natl. Acad. Sci. U.S.A.* **107,** 2598–2603 (2010).

59. Whitehurst, A. W. *et al.* Synthetic lethal screen identification of chemosensitizer loci in cancer cells. *Nature* **446,** 815–819 (2007).

60. Seth, R. B., Sun, L., Ea, C.-K. & Chen, Z. J. Identification and characterization of MAVS, a mitochondrial antiviral signaling protein that activates NF-kappaB and IRF 3. *Cell* **122,** 669–682 (2005).

61. An, H. *et al.* SHP-2 phosphatase negatively regulates the TRIF adaptor protein-dependent type I interferon and proinflammatory cytokine production. *Immunity* **25,** 919–928 (2006).

62. Bellacosa, A. *et al.* Akt activation by growth factors is a multiple-step process: the role of the PH domain. *Oncogene* **17,** 313–325 (1998).

63. Ahn, J.-Y., Hu, Y., Kroll, T. G., Allard, P. & Ye, K. PIKE-A is amplified in human cancers and prevents apoptosis by up-regulating Akt. *Proc. Natl. Acad. Sci. U.S.A.* **101,** 6993–6998 (2004).

64. Tang, X. *et al.* Akt phosphorylation regulates the tumour-suppressor merlin through ubiquitination and degradation. *Nat. Cell Biol.* **9,** 1199–1207 (2007).

65. Matern, H. T., Yeaman, C., Nelson, W. J. & Scheller, R. H. The Sec6/8 complex in mammalian cells: characterization of mammalian Sec3, subunit interactions, and expression of subunits in polarized cells. *Proc. Natl. Acad. Sci. U.S.A.* **98,** 9648–9653 (2001).

66. Vega, I. E. & Hsu, S. C. The exocyst complex associates with microtubules to mediate vesicle targeting and neurite outgrowth. *J. Neurosci.* **21,** 3839–3848 (2001).

67. Fromont-Racine, M., Rain, J. C. & Legrain, P. Toward a functional analysis of the yeast genome through exhaustive two-hybrid screens. *Nat. Genet.* **16,** 277–282 (1997).

68. Bartel, P., Chien, C. T., Sternglanz, R. & Fields, S. *Elimination of false positives that arise in using the two-hybrid system. BioTechniques* **14,** 920–924 (1993).

69. Formstecher, E. Protein interaction mapping: A Drosophila case study. *Genome Research* **15,** 376–384 (2005).

70. Rain, J. C. *et al.* The protein-protein interaction map of Helicobacter pylori. *Nature* **409,** 211–215 (2001).

71. Wojcik, J., Boneca, I. G. & Legrain, P. Prediction, assessment and validation of protein interaction maps in bacteria. *J. Mol. Biol.* **323,** 763–770 (2002).

72. Roland, C. L. *et al.* Inhibition of vascular endothelial growth factor reduces angiogenesis and modulates immune cell infiltration of orthotopic breast cancer xenografts. *Mol. Cancer Ther.* **8,** 1761–1771 (2009).

73. Dineen, S. P. *et al.* Vascular endothelial growth factor receptor 2 mediates macrophage infiltration into orthotopic pancreatic tumors in mice. *Cancer Research* **68,** 4340–4346 (2008).

74. Ou, Y.-H. *et al.* TBK1 Directly Engages Akt/PKB Survival Signaling to Support Oncogenic Transformation. *Molecular Cell* **41,** 458–470 (2011).

75. Zimmermann, M. & de Lange, T. 53BP1: pro choice in DNA repair. *Trends Cell Biol.* (2013). doi:10.1016/j.tcb.2013.09.003

76. Bunting, S. F. *et al.* 53BP1 inhibits homologous recombination in Brca1-deficient cells by blocking resection of DNA breaks. *Cell* **141,** 243–254 (2010).

77. Chapman, J. R., Sossick, A. J., Boulton, S. J. & Jackson, S. P. BRCA1-

associated exclusion of 53BP1 from DNA damage sites underlies temporal control of DNA repair. *J Cell Sci* **125,** 3529–3534 (2012).

78. Sharma, G. G. *et al.* MOF and histone H4 acetylation at lysine 16 are critical for DNA damage response and double-strand break repair. *Mol. Cell. Biol.* **30,** 3582–3595 (2010).

79. Kumar, R. *et al.* Chromatin modifications and the DNA damage response to ionizing radiation. *Front. Oncol.* **2,** 1–9 (2013).

80. Bhoumik, A. & Ronai, Z. ATF2: a transcription factor that elicits oncogenic or tumor suppressor activities. *cc* **7,** 2341–2345 (2008).

81. Ho, H. *et al.* RhoJ Regulates Melanoma Chemoresistance by Suppressing Pathways That Sense DNA Damage. *Cancer Research* **72,** 5516–5528 (2012).

82. Chernikova, S. B., Dorth, J. A., Razorenova, O. V., Game, J. C. & Brown, J. M. Deficiency in Bre1 impairs homologous recombination repair and cell cycle checkpoint response to radiation damage in mammalian cells. *Radiat. Res.* **174,** 558–565 (2010).

83. Blank, M. *et al.* A tumor suppressor function of Smurf2 associated with controlling chromatin landscape and genome stability through RNF20. *Nature Medicine* **18,** 227–234 (2012).

84. Iacopetta, B. TP53 mutation in colorectal cancer. *Hum. Mutat.* **21,** 271–276 (2003).

85. Kubbutat, M. H., Jones, S. N. & Vousden, K. H. Regulation of p53 stability by Mdm2. *Nature* **387,** 299–303 (1997).

86. Schmitt, C. A. *et al.* Dissecting p53 tumor suppressor functions in vivo. *Cancer Cell* **1,** 289–298 (2002).

87. Wood, L. D. *et al.* The Genomic Landscapes of Human Breast and Colorectal Cancers. *Science* **318,** 1108–1113 (2007).

88. Sato, K. *et al.* Histone chaperone activity of Fanconi anemia proteins, FANCD2 and FANCI, is required for DNA crosslink repair. *EMBO J.* (2012). doi:10.1038/emboj.2012.197

89. Zhovmer, A., Oksenych, V. & Coin, F. Two Sides of the Same Coin: TFIIH Complexes in Transcription and DNA Repair. *The Scientific World JOURNAL* **10,** 633–643 (2010).

90. Gupta, A. *et al.* Role of 53BP1 in the Regulation of DNA Double-Strand Break Repair Pathway Choice. *Radiat. Res.* **181,** 1–8 (2014).

91. Wang, B., Matsuoka, S., Carpenter, P. B. & Elledge, S. J. 53BP1, a mediator of the DNA damage checkpoint. *Science* **298,** 1435–1438 (2002).

92. Dellago, H. *et al.* Exo70, a subunit of the exocyst complex, interacts with SNEV(hPrp19/hPso4) and is involved in pre-mRNA splicing. *Biochem. J.* **438,** 81–91 (2011).

93. Lee, I. H. *et al.* Atg7 Modulates p53 Activity to Regulate Cell Cycle and Survival During Metabolic Stress. *Science* **336,** 225–228 (2012).

94. Orvedahl, A. *et al.* Image-based genome-wide siRNA screen identifies selective autophagy factors. *Nature* **480,** 113–117 (2011).

95. Bae, H. & Guan, J. L. Suppression of Autophagy by FIP200 Deletion Impairs DNA Damage Repair and Increases Cell Death upon Treatments

with Anticancer Agents. *Mol. Cancer Res.* **9,** 1232–1241 (2011).

96. Ni, H.-M. *et al.* Dissecting the dynamic turnover of GFP-LC3 in the autolysosome. *Autophagy* **7,** 188–204 (2011).

97. Tasdemir, E. *et al.* Regulation of autophagy by cytoplasmic p53. *Nat. Cell Biol.* **10,** 676–687 (2008).

98. Paull, T. T. *et al.* A critical role for histone H2AX in recruitment of repair factors to nuclear foci after DNA damage. *Molecular Cell* **10,** 886–895 (2000).

99. Onclercq-Delic, R. Possible anti-recombinogenic role of Bloom's syndrome helicase in double-strand break processing. *Nucleic Acids Research* **31,** 6272–6282 (2003).

100. Nakanishi, K. *et al.* Human Fanconi anemia monoubiquitination pathway promotes homologous DNA repair. *Proc. Natl. Acad. Sci. U.S.A.* **102,** 1110–1115 (2005).

101. Henry-Mowatt, J. *et al.* XRCC3 and Rad51 modulate replication fork progression on damaged vertebrate chromosomes. *Molecular Cell* **11,** 1109–1117 (2003).

102. Schlacher, K. *et al.* Double-strand break repair-independent role for BRCA2 in blocking stalled replication fork degradation by MRE11. *Cell* **145,** 529–542 (2011).

103. Petermann, E., Orta, M. L., Issaeva, N., Schultz, N. & Helleday, T. Hydroxyurea-stalled replication forks become progressively inactivated and require two different RAD51-mediated pathways for restart and repair.

Molecular Cell **37,** 492–502 (2010).

104. Baryshnikova, A. *et al.* Synthetic genetic array (SGA) analysis in Saccharomyces cerevisiae and Schizosaccharomyces pombe. *Meth. Enzymol.* **470,** 145–179 (2010).

105. Costanzo, M. *et al.* The genetic landscape of a cell. *Science* **327,** 425–431 (2010).

106. Koh, J. L. Y. *et al.* DRYGIN: a database of quantitative genetic interaction networks in yeast. *Nucleic Acids Research* **38,** D502–7 (2010).

107. Bhoumik, A., Singha, N., O'Connell, M. J. & Ronai, Z. A. Regulation of TIP60 by ATF2 modulates ATM activation. *J. Biol. Chem.* **283,** 17605–17614 (2008).

108. Tang, J. *et al.* Acetylation limits 53BP1 association with damaged chromatin to promote homologous recombination. *Nat. Struct. Mol. Biol.* **20,** 317–325 (2013).

109. Khoronenkova, S. V. & Dianov, G. L. The emerging role of Mule and ARF in the regulation of base excision repair. *FEBS Lett.* **585,** 2831–2835 (2011).

110. Gudjonsson, T. *et al.* TRIP12 and UBR5 suppress spreading of chromatin ubiquitylation at damaged chromosomes. *Cell* **150,** 697–709 (2012).

111. Wang, X. *et al.* HUWE1 interacts with BRCA1 and promotes its degradation in the ubiquitin–proteasome pathway. *Biochem. Biophys. Res. Commun.* (2014). doi:10.1016/j.bbrc.2014.01.075

112. Bhoumik, A. *et al.* ATM-dependent phosphorylation of ATF2 is required for the DNA damage response. *Molecular Cell* **18,** 577–587 (2005).

113. Moyal, L. *et al.* Requirement of ATM-dependent monoubiquitylation of histone H2B for timely repair of DNA double-strand breaks. *Molecular Cell* **41,** 529–542 (2011).

114. Hunt, C. R. *et al.* Hyperthermia activates a subset of ataxia-telangiectasia mutated effectors independent of DNA strand breaks and heat shock protein 70 status. *Cancer Research* **67,** 3010–3017 (2007).

115. Kumar, R. *et al.* Purkinje cell-specific males absent on the first (mMof) gene deletion results in an ataxia-telangiectasia-like neurological phenotype and backward walking in mice. *Proc. Natl. Acad. Sci. U.S.A.* **108,** 3636–3641 (2011).

116. Pierce, A. J., Johnson, R. D., Thompson, L. H. & Jasin, M. XRCC3 promotes homology-directed repair of DNA damage in mammalian cells. *Genes Dev.* **13,** 2633–2638 (1999).

117. Singh, M. *et al.* Lamin A/C Depletion Enhances DNA Damage Induced Stalled Replication Fork Arrest. *Mol. Cell. Biol.* (2013). doi:10.1128/MCB.01676-12

118. Gupta, A. *et al.* Involvement of human MOF in ATM function. *Mol. Cell. Biol.* **25,** 5292–5305 (2005).

119. Pandita, T. K. Role of mammalian Rad9 in genomic stability and ionizing radiation response. *cc* **5,** 1289–1291 (2006).

120. Asaithamby, A. & Chen, D. J. Cellular responses to DNA double-strand breaks after low-dose gamma-irradiation. *Nucleic Acids Research* **37,** 3912–3923 (2009).

121. Zhang, J., Ma, Z., Treszezamsky, A. & Powell, S. N. MDC1 interacts with Rad51 and facilitates homologous recombination. *Nat. Struct. Mol. Biol.* **12,** 902–909 (2005).

122. Hsu, S.-C. *et al.* The Mammalian Brain rsec6/8 Complex. *Neuron* **17,** 1209–1219 (1996).

123. Kee, Y. *et al.* Subunit structure of the mammalian exocyst complex. *Proc. Natl. Acad. Sci. U.S.A.* **94,** 14438–14443 (1997).

124. Yeaman, C. Ultracentrifugation-based approaches to study regulation of Sec6/8 (exocyst) complex function during development of epithelial cell polarity. *Methods* **30,** 198–206 (2003).

125. Steigemann, P. *et al.* Aurora B-mediated abscission checkpoint protects against tetraploidization. *Cell* **136,** 473–484 (2009).

126. Acilan, C., Potter, D. M. & Saunders, W. S. DNA repair pathways involved in anaphase bridge formation. *Genes Chromosomes Cancer* **46,** 522–531 (2007).

127. Schröder-Heurich, B., Wieland, B., Lavin, M. F., Schindler, D. & Dörk, T. Protective role of RAD50 on chromatin bridges during abnormal cytokinesis. *FASEB J.* **28,** 1331–1341 (2014).

128. Thompson, S. L. & Compton, D. A. Proliferation of aneuploid human cells is limited by a p53-dependent mechanism. *The Journal of Cell Biology* **188,** 369–381 (2010).

129. Stetson, D. B. & Medzhitov, R. Recognition of cytosolic DNA activates an IRF3-dependent innate immune response. *Immunity* **24,** 93–103 (2006).

130. Ferguson, B. J., Mansur, D. S., Peters, N. E., Ren, H. & Smith, G. L. DNA-PK is a DNA sensor for IRF-3-dependent innate immunity. *elife* **1,** e00047 (2012).

131. Shimura, T. *et al.* DNA-PK is involved in repairing a transient surge of DNA breaks induced by deceleration of DNA replication. *J. Mol. Biol.* **367,** 665–680 (2007).

132. Kumar, A., Rajendran, V., Sethumadhavan, R. & Purohit, R. CEP proteins: the knights of centrosome dynasty. *Protoplasma* 1–19 (2013). doi:10.1007/s00709-013-0488-9

133. Rogers, K. K., Jou, T.-S., Guo, W. & Lipschutz, J. H. The Rho family of small GTPases is involved in epithelial cystogenesis and tubulogenesis. *Kidney Int.* **63,** 1632–1644 (2003).

134. Liu, Q. *et al.* The proteome of the mouse photoreceptor sensory cilium complex. *Mol. Cell Proteomics* **6,** 1299–1317 (2007).

135. Pan, J., Wang, Q. & Snell, W. J. Cilium-generated signaling and cilia-related disorders. *Lab. Invest.* **85,** 452–463 (2005).

136. O'Driscoll, M., Ruiz-Perez, V. L., Woods, C. G., Jeggo, P. A. & Goodship, J. A. A splicing mutation affecting expression of ataxia-telangiectasia and Rad3-related protein (ATR) results in Seckel syndrome. *Nat. Genet.* **33,** 497–501 (2003).

137. Valdes-Sanchez, L. *et al.* ATR localizes to the photoreceptor connecting cilium and deficiency leads to severe photoreceptor degeneration in mice. *Human Molecular Genetics* **22,** 1507–1515 (2013).

138. Ben Fogelgren *et al.* The Exocyst Protein Sec10 Interacts with Polycystin-2 and Knockdown
Causes PKD-Phenotypes. *PLoS Genet.* **7,** e1001361 (2011).

139. Stiff, T. *et al.* Deficiency in origin licensing proteins impairs cilia formation: implications for the aetiology of Meier-Gorlin syndrome. *PLoS Genet.* **9,** e1003360 (2013).

140. Kalay, E. *et al.* CEP152 is a genome maintenance protein disrupted in Seckel syndrome. *Nat. Genet.* **43,** 23–26 (2010).

141. Griffith, E. *et al.* Mutations in pericentrin cause Seckel syndrome with defective ATR-dependent DNA damage signaling. *Nat. Genet.* **40,** 232–236 (2007).